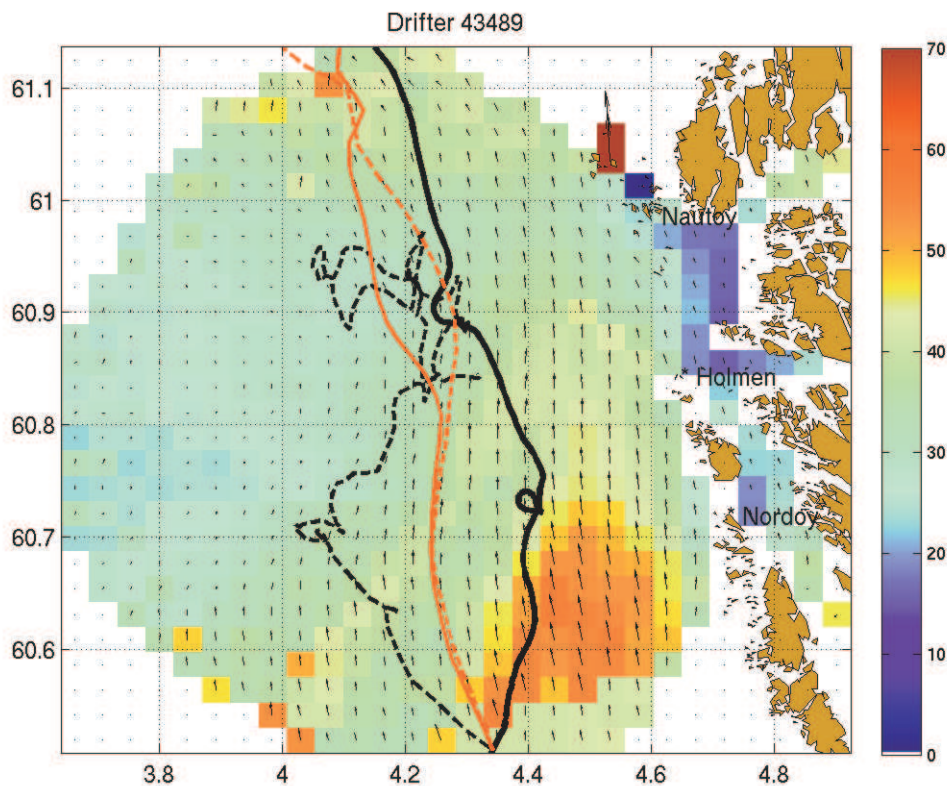# An assessment of HF radar current measurements in Norwegian waters

Øyvind Breivik, Knut-Frode Dagestad*, Morten W. Hansen* and Johnny A. Johannessen*

Drifter 43489

*Nansen Environmental and Remote Sensing Center

report

Title	Date
An assessment of HF radar current measurements in Norwegian waters	2009-05-20
	Report no. 2009/08

Author(s)	Classification
Øyvind Breivik[1], Knut-Frode Dagestad[2], Morten W. Hansen[2] and Johnny A. Johannessen[2]	☑ Free ☐ Restricted **ISSN** 1503-8025
[1] Norwegian Meteorological Institute, [2]Nansen Environmental and Remote Sensing Center	

Client	Client's reference
StatoilHydro ASA	**Contract no 4501607903**

Abstract

A comparison of Fedje HF radar measurements against surface drifters and SAR images and SAR Doppler current measurements is performed. The results indicate that the radial current vectors correlate well with drifter data (r ranges from 0.7-0.9) and show qualitative agreement with SAR Doppler current and roughness images. The total vectors yield significantly lower correlation indicating that the algorithm for combining radial current components into total vectors requires some improvement. Theoretical coverage maps for two regions in the north of Norway are presented along with operational recommendations.

Keywords

HF radar, SAR, drifters, Norwegian Coastal Current

Disiplinary signature	Responsible signature
Magnar Reistad	**Karen H Doublet**

1 Introduction

Measuring surface currents using high-frequency (HF) radars is a technique well established through numerous operational and research-oriented radar networks around the world, most notably along the West coast and the Eastern seaboard of the USA. A pre-operational real-time system was deployed at Fedje on the west coast of Norway during a campaign in 2000 (see Breivik and Sætra, 2001, Essen *et al*, 2003). Since 2005 an operational HF radar network has been in place around Fedje (see http://hf.met.no). Here we present an assessment of the precision of this network of radars based on a comparison with a limited dataset of surface drifters and a more extensive dataset of satellite measurements.

The study draws conclusions regarding the precision of the existing radar network and makes some recommendations regarding the usefulness of deploying similar radar networks in two specific regions in Northern Norway.

2 Averaged HF radar current fields

The current vectors from the HF radars (CODAR) are computed at a fixed spatial grid with 2.5 km resolution. The hourly fields (http://hf.met.no) exhibit large spatial and temporal variability due to mesoscale current variability as well as changes in wind drag and tidal motion. To filter out the temporal variations, we have averaged the currents over time, with vectors averaged by components and speed averaged as a scalar value. Mean vectors are defined as

$$[\langle U \rangle, \langle V \rangle],$$

while the average speed is the root-mean-square of the current vector

$$\langle \sqrt{U^2 + V^2} \rangle.$$

The brackets denote ensemble averages. The averaged speed and vectors for the years 2006 (starting from 29 July) to 2008 are shown in Figure 1-Figure 3. The flow pattern is very similar for all years, with a northwards "jet" of width of 20-40 km close to the coast, and a typical speed of 40-60 cm/s. The higher average speed for 2006 may be explained by the fact that mainly autumn/winter months with generally stronger current are used. Averages for each calendar month for the period 2006-2008 are found in Appendix A. The pattern is also seen to vary only slightly throughout the year. The average speed is at a minimum in April to June, with an increase from July and a maximum in October. The speed decreases again from February-March. For the autumn and winter months with strongest current, the direction is also more directly towards north than in spring and summer.
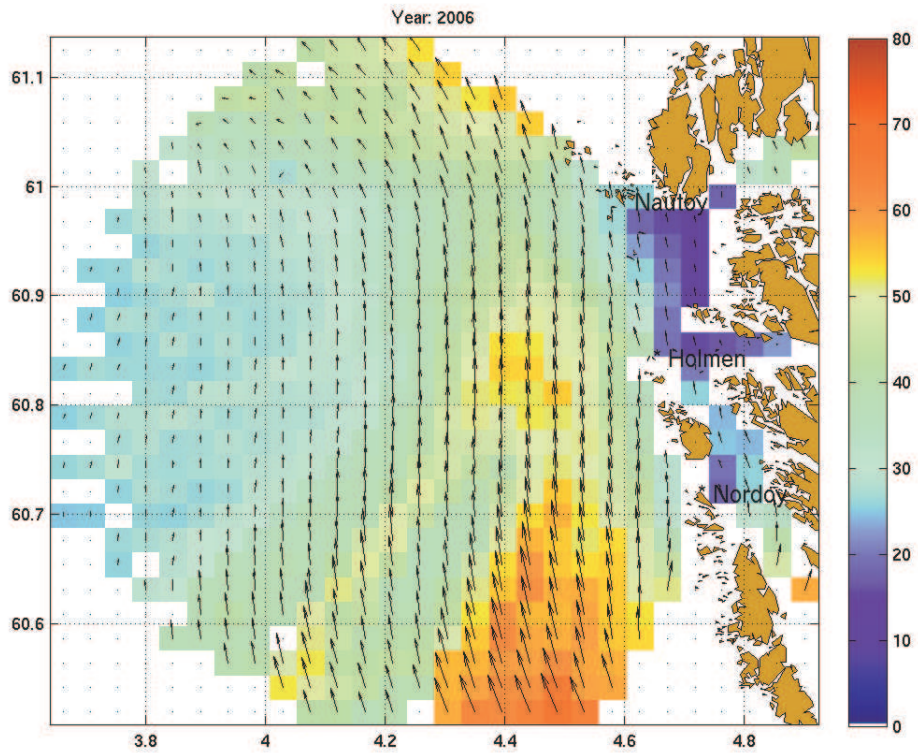
Figure 1: CODAR current at Fedje averaged for the period 29 June – 31 Dec 2006. The colour scale indicates current speed [cm/s]. The overlaid vectors are obtained by averaging the eastward and northward components in time. The three radars are marked from south to north as "Nordoy", "Holmen" and "Nautoy".
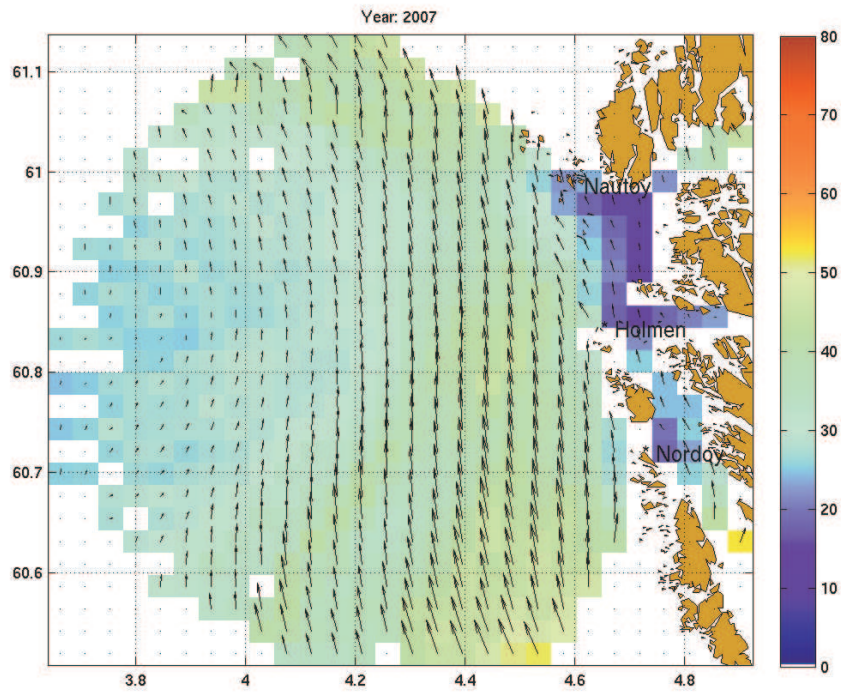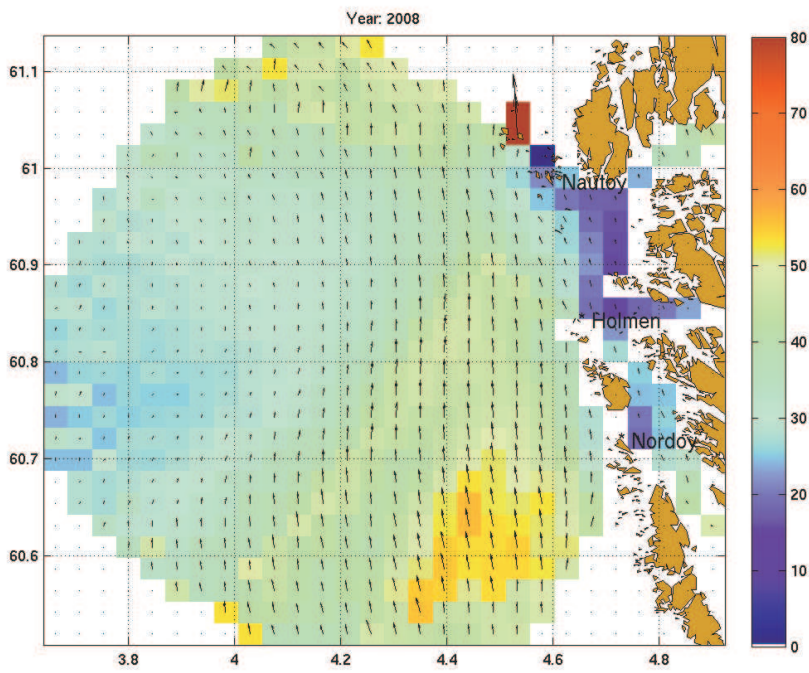
Figure 2: Average current field for 2007.

Figure 3: Average current field for 2008.

3 Distributions of HF radar speed and directions

To investigate the spatial and temporal distributions of speed and directions we have selected 7 points (grid cells), as seen in Figure 4.
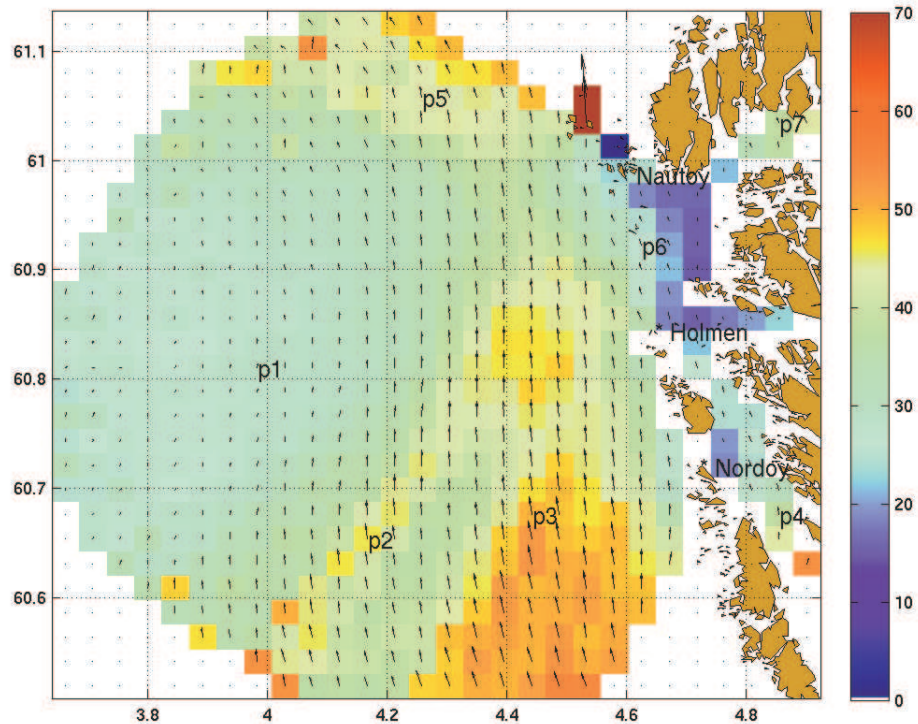

Figure 4: Location of 7 positions (p1-p7) where temporal distribution of current speed and directions are investigated. The background colour and arrows are the CODAR current averages from 29 June 2006 to 31 Dec 2008.

The distribution of CODAR speed for the 7 points is seen in Figure 5. All histograms show natural and smooth distributions, with most frequent speeds between 20 and 50 cm/s for the various locations.
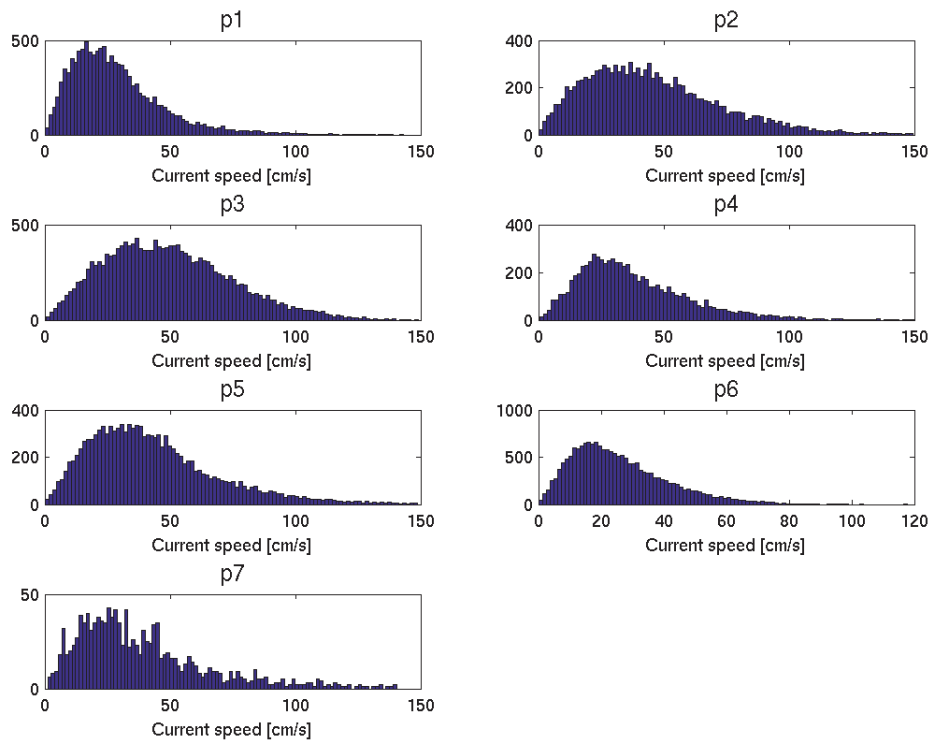
Figure 5: Histograms of CODAR current speed for the 7 locations shown in Figure 4. No outliers have been removed.

The distribution of current directions for the same locations is shown in figures in Appendix B.

4 Radar-drifter comparison

A comparison of current maps from the HF radars located at Fedje with nine self-locating datum marker buoys (SLDMB) deployed between 31 March and 4 April (referred to hereafter as the drifters). drifters deployed during a field campaign in April 2008 has been carried out. Trajectories from the drifters are shown in Figure 6. The drifters displayed a range of speeds and directions during their transit through the radar area, but the overall drift direction was unsurprisingly toward the north. Two different approaches have been pursued in comparing drifter data and radar measurements. The first is a direct comparison of current vectors estimated from the drifter trajectories with the nearest HF radar measurements. The second method is a comparison of the drifter trajectories and synthetic trajectories estimated from the radar currents.
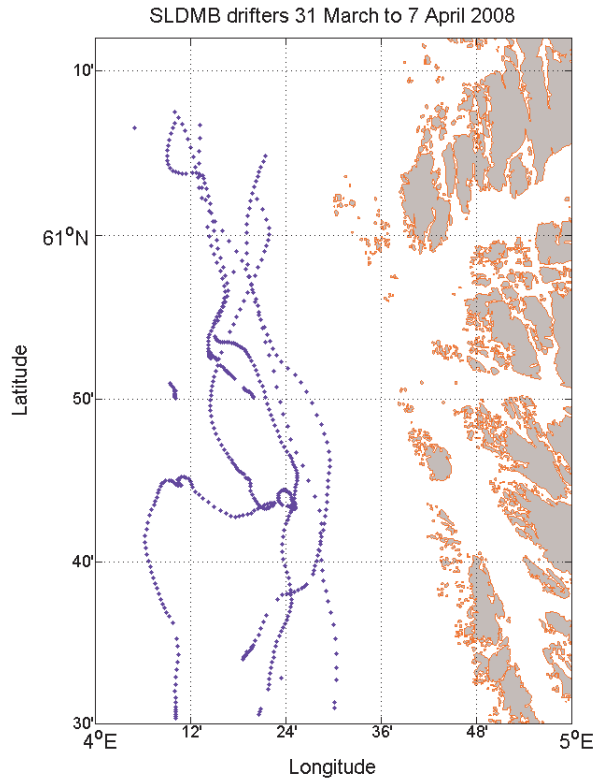
Figure 6: Drifter trajectories from the field campaign. Only GPS positions within radar coverage are shown.

4.1 Current vector comparison

A total of 571 current vectors were estimated from the drifter trajectories that fall within the HF radar coverage (at least two radar measurements within 3 km range). The overall correlation with the total vectors produced by the three radars is rather poor (r=0.48, see Figure 7). From Table 1 we see that the northward mean absolute deviation is on the order of 17 cm/s. This amounts to more than 50% of the average speed. The speed distribution on the other hand is quite reasonable, as the quantile-quantile plot in Figure 8 illustrates. The quantile-quantile plot juxtaposes measurements of similar cumulative probability, *i.e.*, values which are equally likely to be exceeded.

Figure 7: Correlation between northward velocity *v* of drifters (SLDMB) and radar (CODAR).

Figure 8: Quantile-quantile plot of speed of drifters (SLDMB) and radar current (CODAR). The quantile-quantile plot juxtaposes measurements of similar cumulative probabil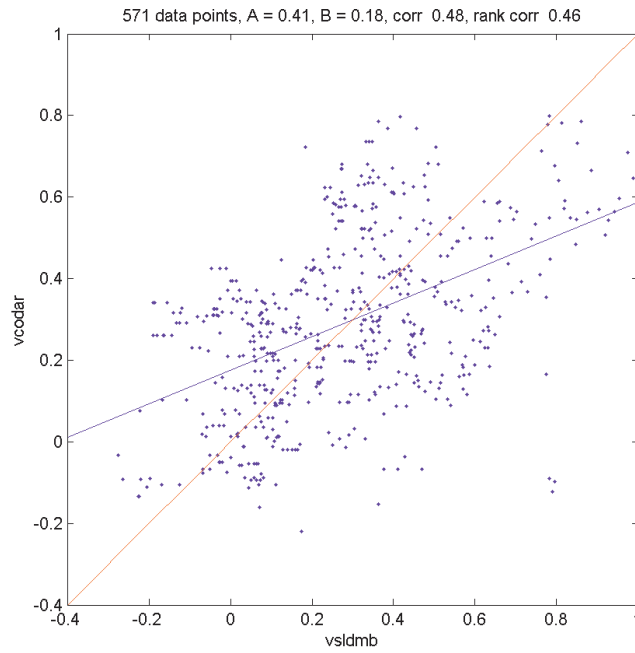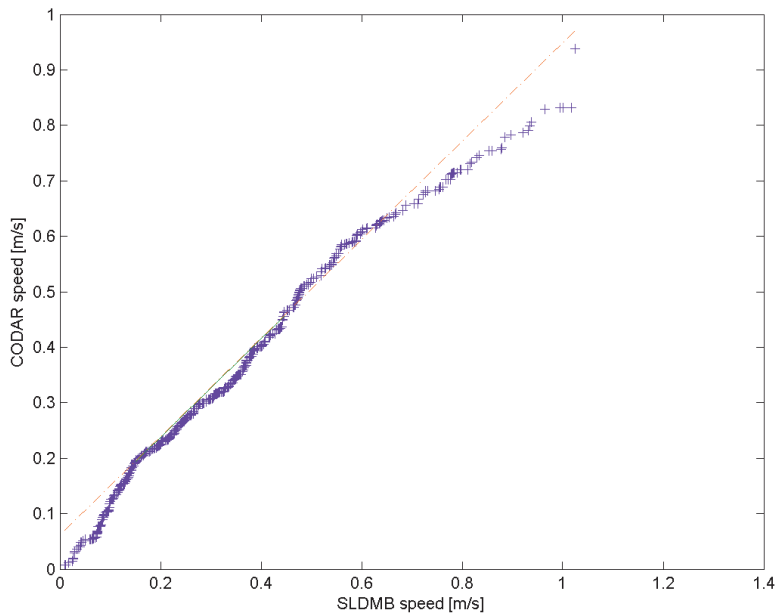ity, *i.e.*, values which are equally likely to be exceeded. As can be seen the distribution is comparable over the range of speeds observed, but the radars underestimate the speed somewhat.

		Total vectors		Nordøy	Holmen Grå	Nautøy
		$N=571$		$N=1922$	$N=864$	$N=1958$
		East comp.	North comp.	Radial components		
Drifters	average	–3	27	–9	10	10
	median	–3	27	–7	18	9
Codar	average	–4	29	–4	10	16
	median	–2	28	–2	14	15
Comparison	Root-mean-square deviation	19	24	21	15	22
	Bias (Drifter-Codar)	–2	2	–5	0	6
	Median absolute deviation	9	17	11	10	13
	Correlation		0.48	0.71	0.90	0.72

Table 1: Comparison of drifter and radar velocities. The first two numerical columns compare the east and north components of matching drifter and radar vectors; the last three columns compare the drifter and radar velocities in the radial direction for each of the three radars. All velocities are given in cm/s.

However, a more robust estimate of the quality of the radar measurements is a comparison of the original *radial* measurements of each individual radar against the drifter velocity. We have decomposed the current vectors derived from the drifter trajectories in radial components toward or away from each radar (Nordøy, Holmen Grå and Nautøy) and compared the resulting radial vectors against the radial vectors from the individual radars. The radial component of the current vector toward the radar is given by

$$u_r = u \sin\theta + v \cos\theta,$$

where u is the east component and v is the north component of the current vector while θ is the direction toward the radar, measured clockwise from north. The results are shown in Table 1 and Figure 9. The correlation is significantly higher than for the total vectors derived from a combination of these radial currents. The Holmen Grå site shows remarkably high correlation ($r = 0.90$) with the drifter data, whereas the two other radars display some bias (see Table 1). The average deviation is now 10-13 cm/s, significantly lower than the 17 cm/s found for the total vectors. This suggests that the individual radars are measuring the surface current well, but that the algorithm used to derive total vectors from a linear combination of the nearest radial measurements has certain weaknesses.
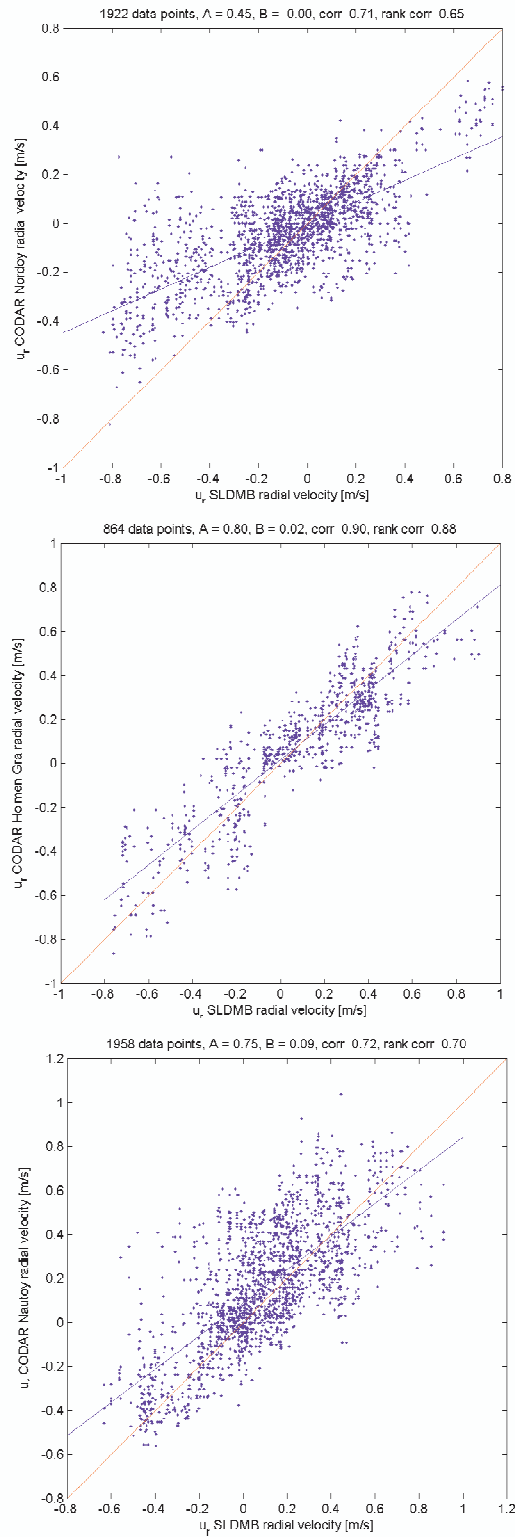
Figure 9: Correlation between radial velocities of drifters (SLDMB) and Codars at Nordøy (top), Holmen Grå (middle) and Nautøy (bottom).

4.2 Drifter trajectories versus synthetic radar trajectories

We have compared synthetic trajectories computed from the radar current fields with the trajectory of the 5 buoys that were within the radar coverage area for the longest period. The trajectories are shown in Figure 10-Figure 14. Also shown are three synthetic trajectories obtained by forward integration using the HF radar current fields. Integration using hourly updated CODAR fields is seen to be unstable, and the trajectories deviate strongly from the drifter trajectory for several of the cases. Much better and more stable agreement with the drifter trajectories is obtained by using radar current fields averaged over the period for which the drifter is within radar coverage and the 7 days prior to start of integration.
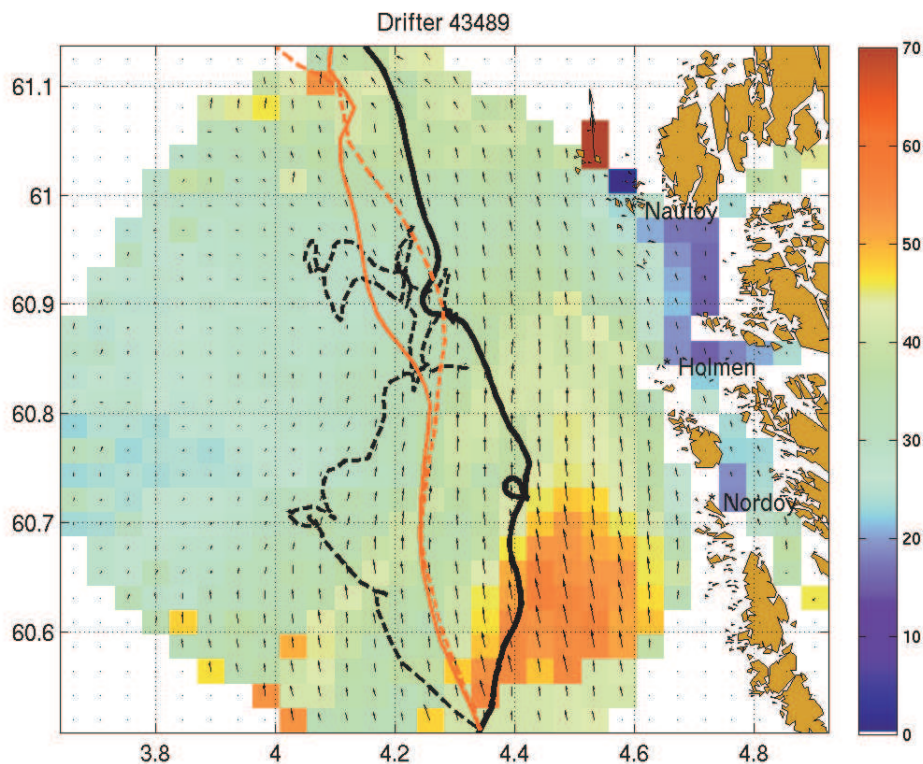

Figure 10: Comparison of trajectory of drifter number 43489 (solid black line) with CODAR current. The dashed black line shows the trajectory obtained by forward integration by using hourly updated CODAR vectors. The red dashed trajectory is obtained by using the CODAR current averaged over the period for which the drifter was within the CODAR coverage area. The solid red trajectory is obtained by using the mean CODAR field for the previous 7 days for integration. Averaged radar speed (colour) and direction (arrows) is shown as background.
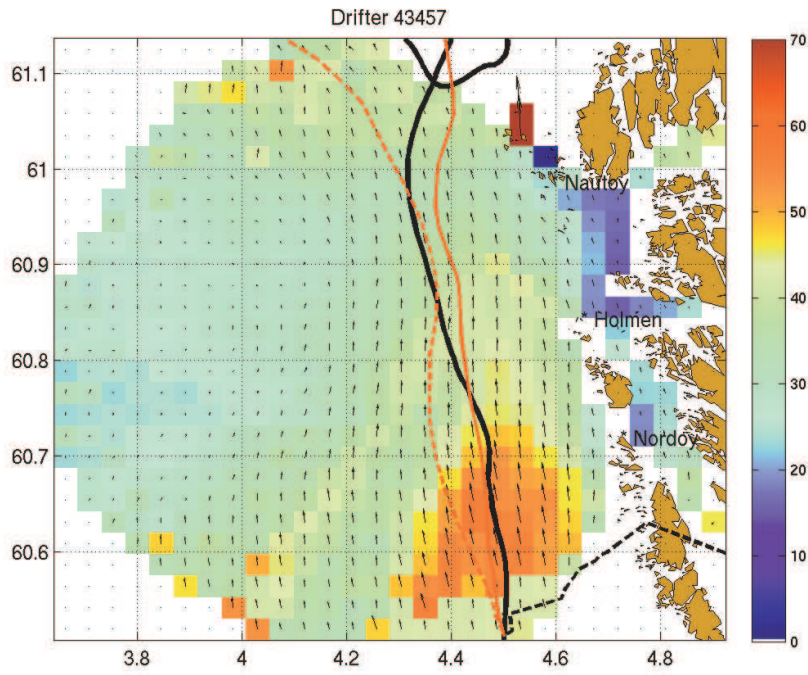
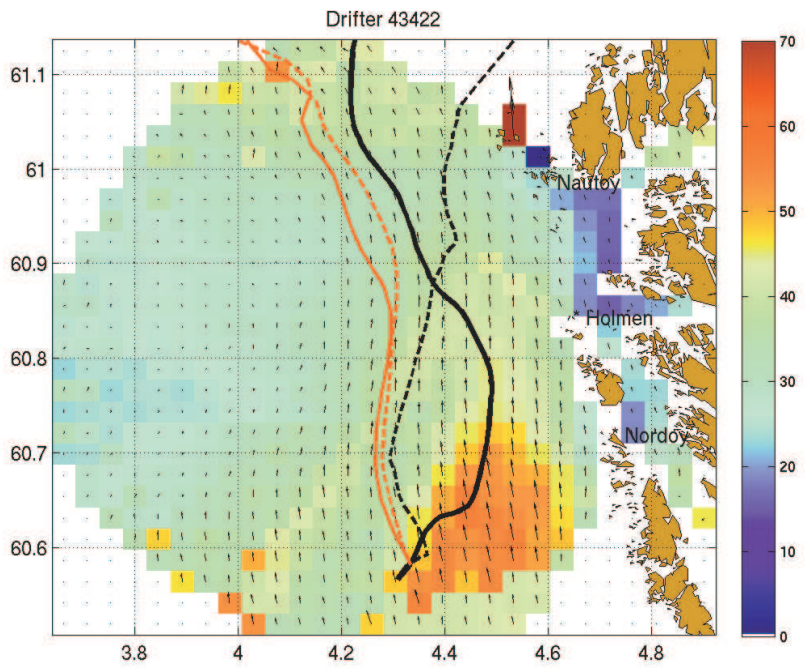**Figure 11: Same as Figure 10, but for drifter number 43457.**

Figure 12: Same as Figure 10, but for drifter number 43422.
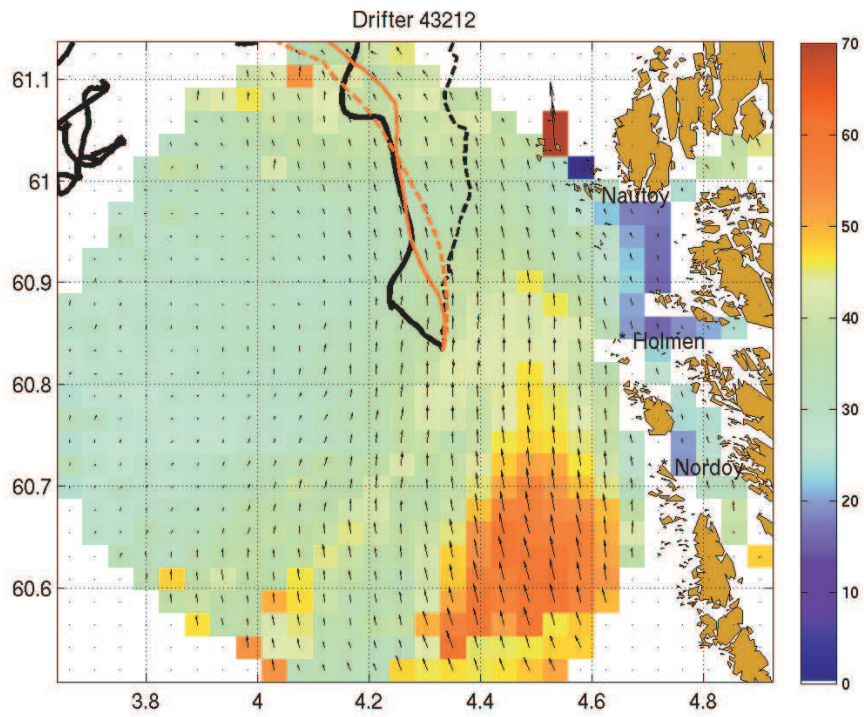
Figure 13: Same as Figure 10, but for drifter number 43212.
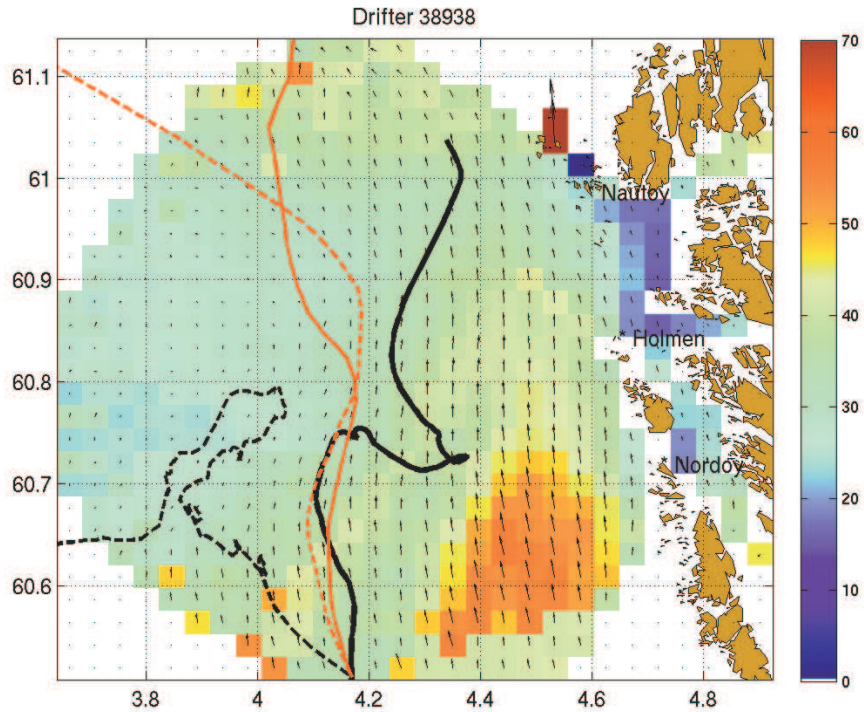

Figure 14: Same as Figure 10, but for drifter number 38938.

5 Ocean surface current observed with Synthetic Aperture Radar

The ability to detect ocean surface current fronts and eddies with Synthetic Aperture Radars (SAR) at a high resolution (~100 m) has been recognised for more than 20 years. SAR sensors are sensitive to ocean surface roughness at a scale of a few centimetres, and this roughness is modulated by the interaction of gradual or rapidly changing surface currents with longer ocean waves. The SAR image outside South-Western Norway on Figure 15 is one example very rich in structures depicting the meandering coastal current, where dark areas (low radar backscatter) correspond to surface divergence and brighter areas correspond to surface convergence, according to the classical interpretation (Johannessen *et al*, 2005). A different mechanism through which surface current fronts and eddies can be indirectly observed with SAR is by collection of thin biological films which can dampen the surface roughness. This mechanism is however only effective for very low wind speeds (below 5-7 m/s), and it shows typically the history of the currents.
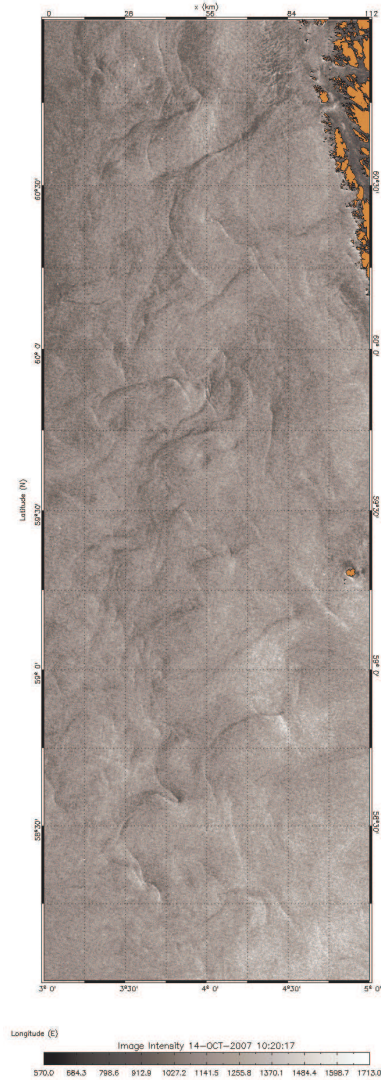
Figure 15: Envisat ASAR roughness image showing strong meandering pattern of the Norwegian Coastal Current off the west coast of Norway. Image is generated with SARTool software, courtesy of Fabrice Collard, CLS, France.

Although the understanding and interpretation of the SAR surface current imaging mechanism has been strengthened over the years, a challenge has remained to extract quantitatively the two dimensional surface current field from its observed modulation of the small scale ocean roughness. One important step forward was made with the paper of Chapron *et al.* (2005) where it was shown that by careful analysis of the raw SAR signals, it was possible to extract quantitatively the ocean surface velocity in one dimension, towards/away from the sensor. The principle is the same as for the speed-measuring laser-pistols used by the police, where velocity of the target is calculated from the Doppler shift of the return signal.

The Envisat ASAR based Doppler velocity is given at a resolution of ~5 km, which is coarser than the detected roughness field (Figure 15), but still close to the resolution of coastal HF-radars, and with a much larger coverage, with typically 400 km width of the satellite swath. The orbital motion of wind generated waves makes a large contribution to the SAR measured surface Doppler velocity, and a remaining nontrivial task is to subtract this contribution to extract the desired ocean surface current. The relative surface Doppler velocity is first calculated, and the absolute velocity is calculated after adjusting the zero-level of motion to the Doppler frequency over land, which is not moving relative to the fixed Earth. Determination of the correct zero-level may be a challenge, in particular for a complex coastline such as the Norwegian, and hence the Doppler velocity scale might be biased. An overview of the present status of SAR current retrieval using Doppler is given in Johannessen *et al*. (2008).

5.1 SAR monitoring of the Fedje HF radar domain

Data from Envisat ASAR (Advanced SAR) are downloaded at NERSC, and an automated system is set up to routinely collect and compare SAR measured roughness and Doppler velocity with surface current vectors from the CODAR system at Fedje. Roughness images at a resolution of 150 m, overlaid CODAR surface current vectors are made available at http://sat.nersc.no/fedje. More than 370 scenes have been collected, and for scenes after May 2008 an image showing the surface Doppler velocity is also available for all SAR scenes in addition to the roughness image. For this product, CODAR current vectors projected in the SAR look direction are overlaid for direct comparison.

5.2 Comparison of HF radar vectors with Envisat ASAR roughness and Doppler velocity

For several scenes with low wind, CODAR current vectors are seen to align closely with bands of surface slicks which dampen the short surface waves. One example is shown in Figure 16. This verifies the slicks observed with SAR as reliable indicators of surface currents, although they represent the recent history of the surface current, rather than the instantaneous surface current, mapped with the CODAR and SAR Doppler. Since the surface current field changes within the time it takes to align and redistribute the surface slicks, an exact agreement with the CODAR vectors cannot be expected. Such comparison also validates qualitatively the performance of the CODAR for cases with low wind speed.
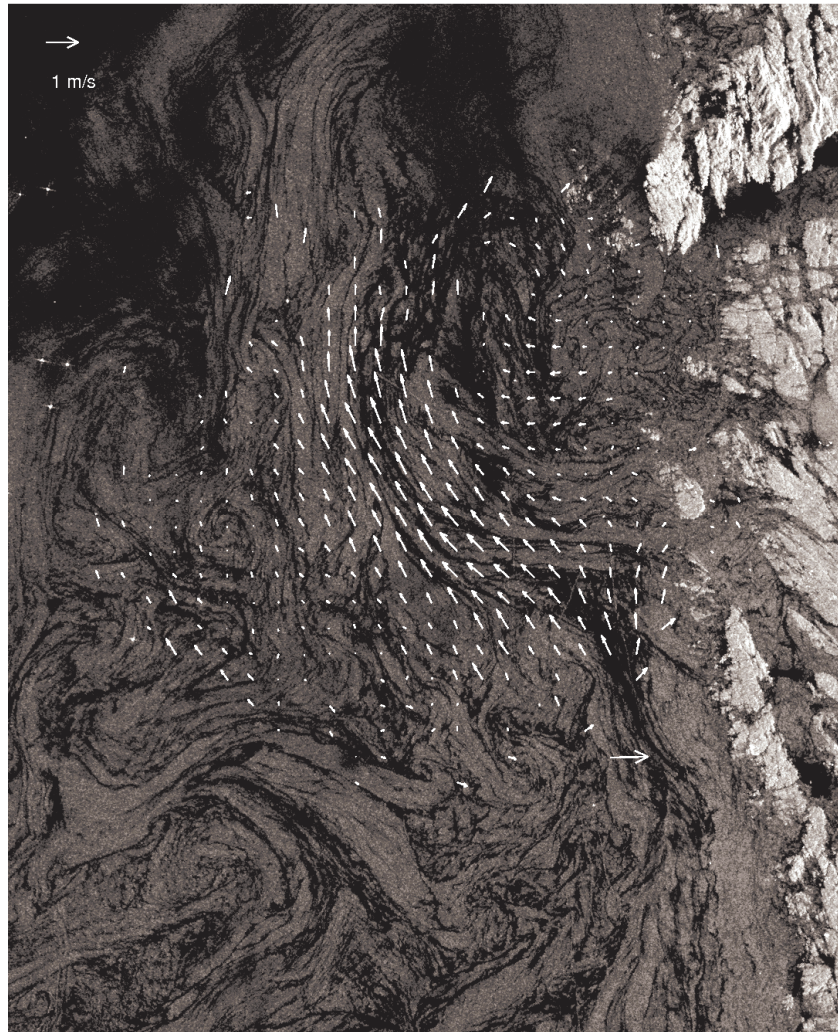
Figure 16: An Envisat SAR roughness image from 8 May 2008, 10:12 UTC, off the coast of Fedje. The dark bands on the image are interpreted as areas where natural surface slicks (e.g. biogenic oils) are collected and redistributed by the surface current. The white arrows are the surface current measurements from the CODAR for the nearest hour, with the scale displayed in the upper left.

When the wind is above ~5-7 m/s, thin surface slicks are generally not able to dampen the surface waves, but roughness modulations due to wave-current or wave-wave interaction may be displayed as brighter or darker anomalies, as proposed by Johannessen *et al*. (2005) and shown on Figure 15. When comparing such Envisat ASAR roughness images with CODAR current vectors from Fedje, we find some qualitative agreement in several cases, but not as tight a relation as expected. One example is shown on Figure 17. Some of the CODAR current vectors seem to be aligned with a meandering current as indicated by dark and bright SAR roughness anomalies, but several other vectors seem less correlated. One possible explanation could be that the HF radar current vectors are generally of lower accuracy along the boundary of the coverage, and where the angles towards the HF-radar antennas are aligned, such as between the antennas close to the coast. Also for the case shown in Figure 16, the HF radar vectors along the boundary

seemed to be less oriented along the surface current as indicated by surface slicks on the SAR roughness image. A second possible explanation might be that the convergence/divergence patterns observed by SAR occur in zones which are too narrow to have much influence on the CODAR, which averages the current over areas of approximately 2.5x2.5 km.
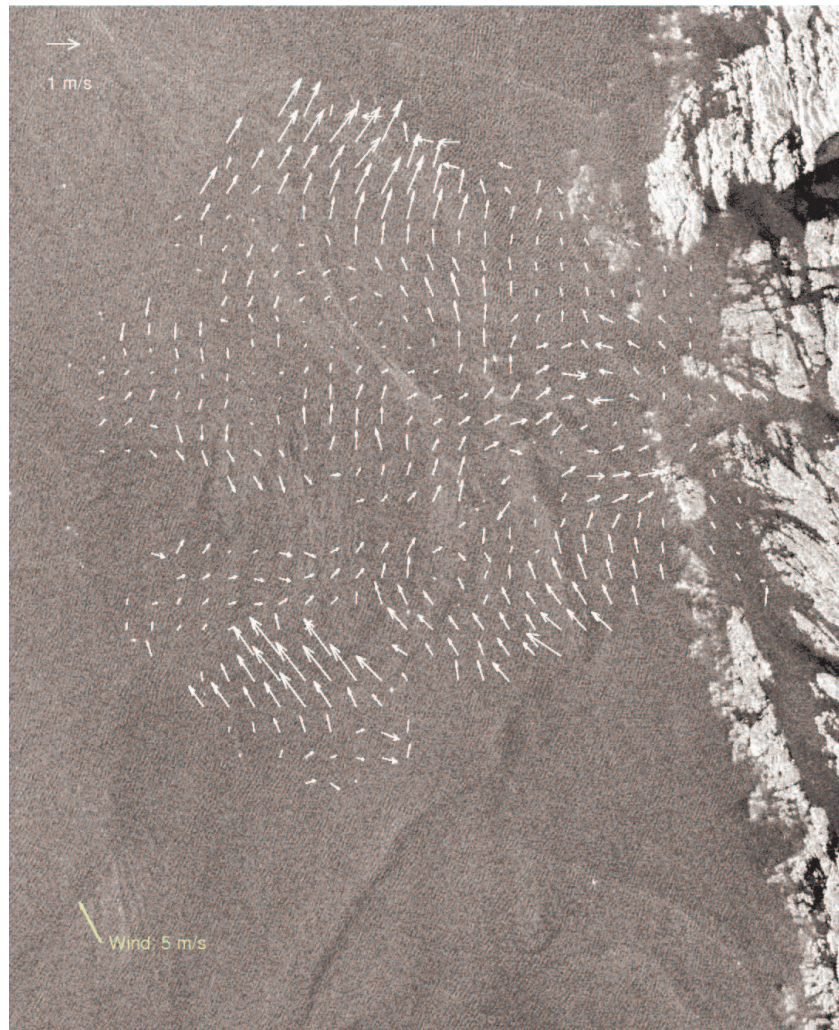

Figure 17: Envisat ASAR roughness image from 24 December 2008, 21:10 UTC, overlaid CODAR current vectors for the nearest hour. Wind speed and direction from the NCEP GFS model is indicated with the yellow arrow.

In some scenes with very strong wind, the HF radar current vectors seem to align with the wind, indicating a wind generated surface current. One such example is shown on Figure 18. The SAR brightness image shows a sharp wind front, probably a low pressure centre, and CODAR current vectors follows closely the wind direction, which is evident from the SAR image although no forecast models are accurate enough to verify the wind pattern. The corresponding SAR Doppler velocity image (right part of Figure 18) shows very good agreement, with positive values where the wind and HF radar current are in the SAR look direction, and vice versa. It should be noted that the SAR Doppler velocity also

contains a contribution from the orbital motion of the wind waves which cannot be easily subtracted. The HF radar current should contain no such contribution since the view angle is horizontal. On the other hand, the wave induced surface current (Stokes drift) may give a contribution in addition to the underlying current.

Figure 18: An Envisat ASAR roughness image (left) from 6 February 2008 10:04 UTC, showing a very sharp wind front. The right image shows the Doppler surface velocity for the same scene, where the arrow indicates the direction of positive Doppler (satellite look direction). The orange maxima to the west of the front corresponds to a positive (aligned with black arrows) surface velocity of 1m/s and the blue minima to the east of the front corresponds to a negative surface velocity of 2m/s. The white arrows are the surface current measurements from the CODAR for the nearest hour.

In cases with moderate wind speed, the correlation between SAR Doppler velocity and HF radar currents is often not as evident as in Figure 18. One example is shown on Figure 19. Here the ASAR surface Doppler velocity is compared with HF radar current vectors projected onto the direction of positive Doppler velocity. For most of the scene an overall good agreement is found both qualitatively and quantitatively, with eastwards current of ~0.5 m/s in the western (left) part, and westwards currents of about the same magnitude closer to the coast. The ASAR Doppler velocity shows slightly higher speed, but this may be explained by the fact that the orbital motion of waves contribute in addition to the surface current. In between the easterly and westerly currents is a zone with weak currents seen both in the HF radar field and the SAR Doppler image (grey values). Two

regions where the HF radar current vectors differ from the SAR Doppler velocity are marked with red contours. They are located respectively close to the boundary of the HF radar coverage and close to the coast (*i.e.* between radar antennas), and may therefore have lower confidence, as argued above.
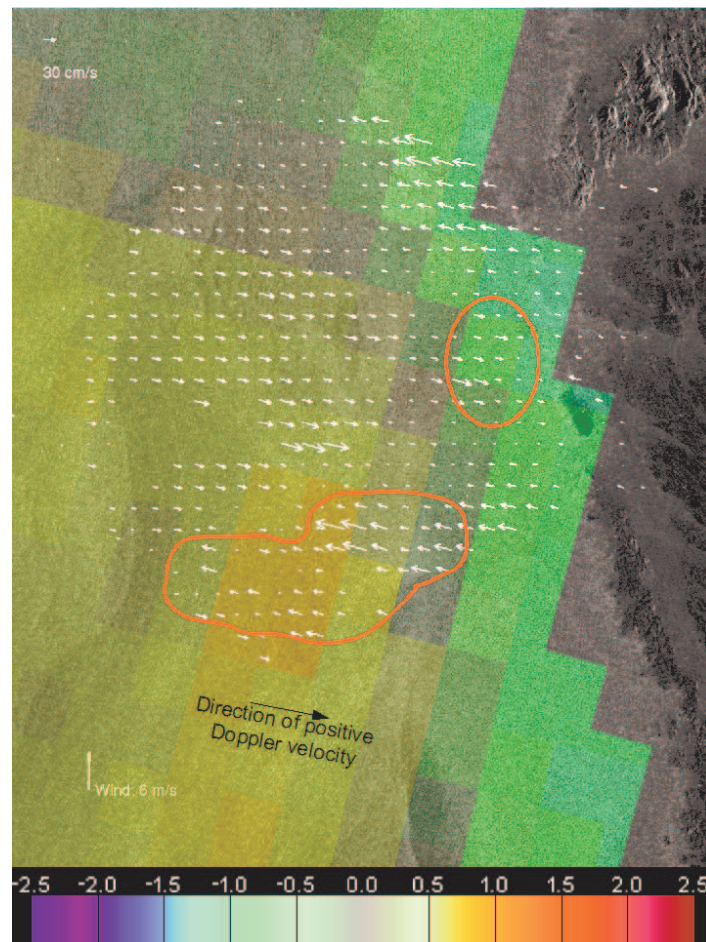

Figure 19: Envisat ASAR roughness image (greyscale) overlaid surface Doppler velocity (colour scale m/s) for the same scene and HF radar current vectors which are projected into the direction of positive Doppler velocity (black arrow). The SAR image is acquired 26 December 2008 10:21 UTC, and the HF radar measurements are from the nearest hour. Wind speed and direction from the NCEP forecast model is indicated with the yellow arrow in the lower left.

Another example is shown on Figure 20. Here the SAR Doppler velocity is mainly positive (eastwards), whereas the HF radar current vectors have also a component in the opposite direction for part of the area. However, there is still a correlation, and if ~1 m/s is subtracted from the SAR Doppler velocity, the agreement would be better. This indicates that in this case the absolute reference level of the Doppler velocity is wrongly estimated (see discussion above). As for the case in Figure 19, the HF radar vectors on the boundary (in particular the southernmost vectors) seem to disagree more with the SAR Doppler.
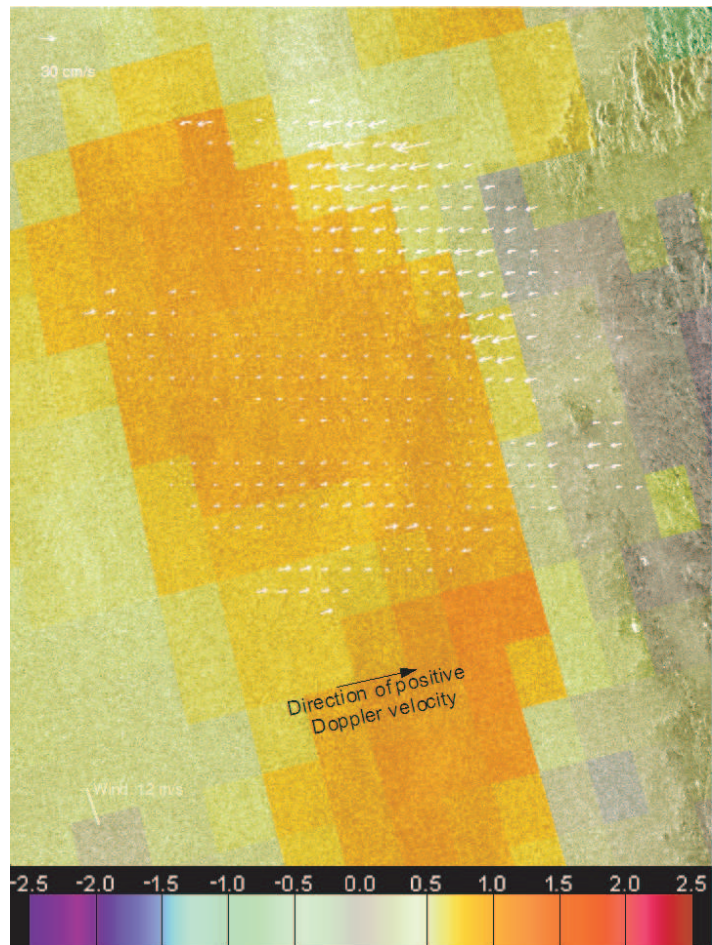
Figure 20: Same as Figure 19, but for a scene from 6 January 2009 21:02 UTC.

In several other cases, very low correlation is found between HF radar vectors, ASAR roughness and Doppler velocity. Often this seem to be due to a chaotic wind field, which may disturb all three measurements, without being stable enough in space and time to induce a noticeable surface current. An example is given in Figure 21, where the SAR roughness reveals a messy wind field. These roughness variations are signatures of wind, and not of surface currents, and hence agreement with HF radar vectors cannot be expected. The effect of the wind on the SAR Doppler velocity could be compensated for if the wind field was known, but it remains a challenge.

Figure 21: Example of Envisat ASAR roughness image with chaotic wind signatures, from 30 Dec 2008 21:21 UTC.

5.3 Detectability of ocean currents at Fedje by SAR Doppler

The accuracy of the SAR radial Doppler velocity is on the order of 20-30 cm/s, and thus a current must have a component of at least this strength in the SAR look direction to be reliably detected. The CODAR current may be used to check this. The components of the CODAR current projected in SAR look direction for ascending and descending satellite tracks are shown in Figure 22 and Figure 23, respectively. It is seen that the components in the SAR look direction are generally below or close to the noise level. Thus the main northward flow at Fedje is unfavourable, since the satellite look directions are more close to eastwards and westwards at this latitude.
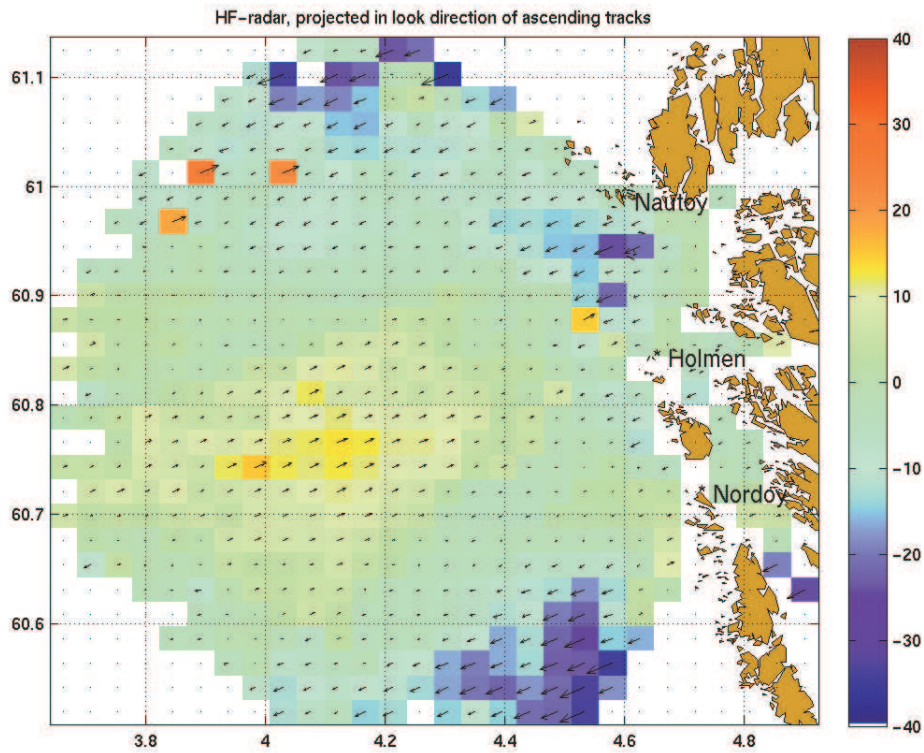
Figure 22: Averaged CODAR vectors projected in the SAR look direction for ascending (northwards) satellite tracks. Only data collocated in time with 31 Envisat ASAR overpasses in 2008 are used. The background colour indicates the magnitude of the CODAR speed in this direction, and the arrows indicate the direction of positive Doppler velocity. The unit of the colour bar is cm/s.
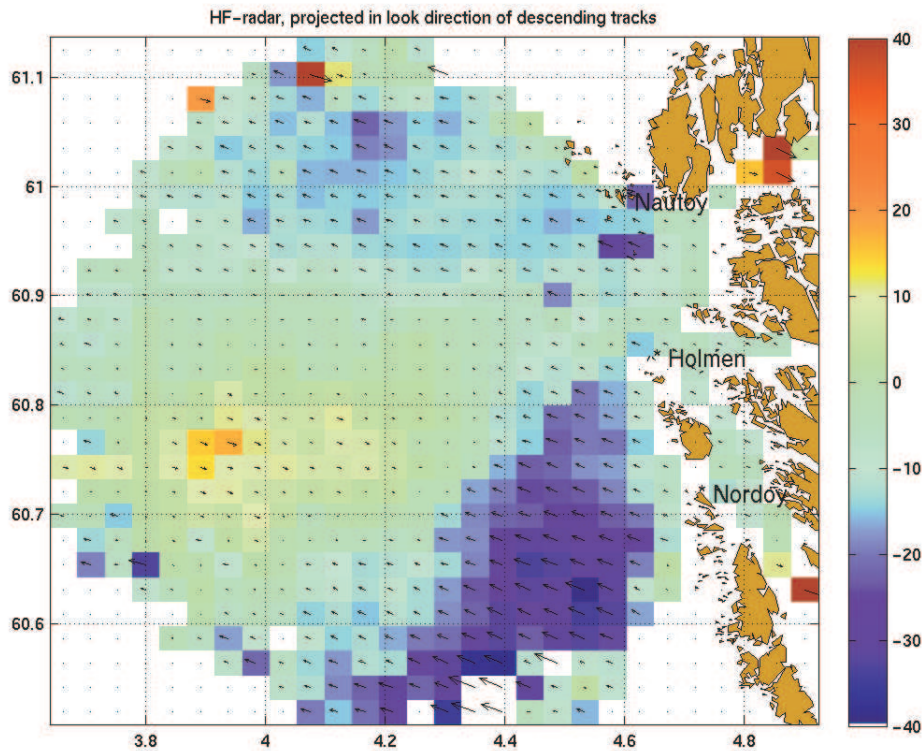
Figure 23: Same as Figure 22, but for 29 descending (southwards) satellite tracks from 2008.

Nevertheless, a reconstruction of the 2-dimensional current field at Fedje may be attempted by combining the mean Doppler velocity for ascending and descending satellite passes. The mean ASAR surface Doppler velocity for 50 ascending and 50 descending satellite passes are shown on Figure 24. These Doppler velocities contain contribution from both wind-waves and current, but the Codar measurements can in this case be used to correct for the wind-wave contribution. As can be seen in Figure 4, the mean HF radar current around 003.8-004.0° E and 60.7-60.9° N is very small. The ascending Doppler velocity is also very small at this location, indicating that the contribution from wind has averaged out, whereas the descending Doppler velocity is here positive with a value of ~25 cm/s. As a rough correction, this constant value is subtracted from the mean ascending Doppler velocity, assuming that this is the mean contribution from the wind.
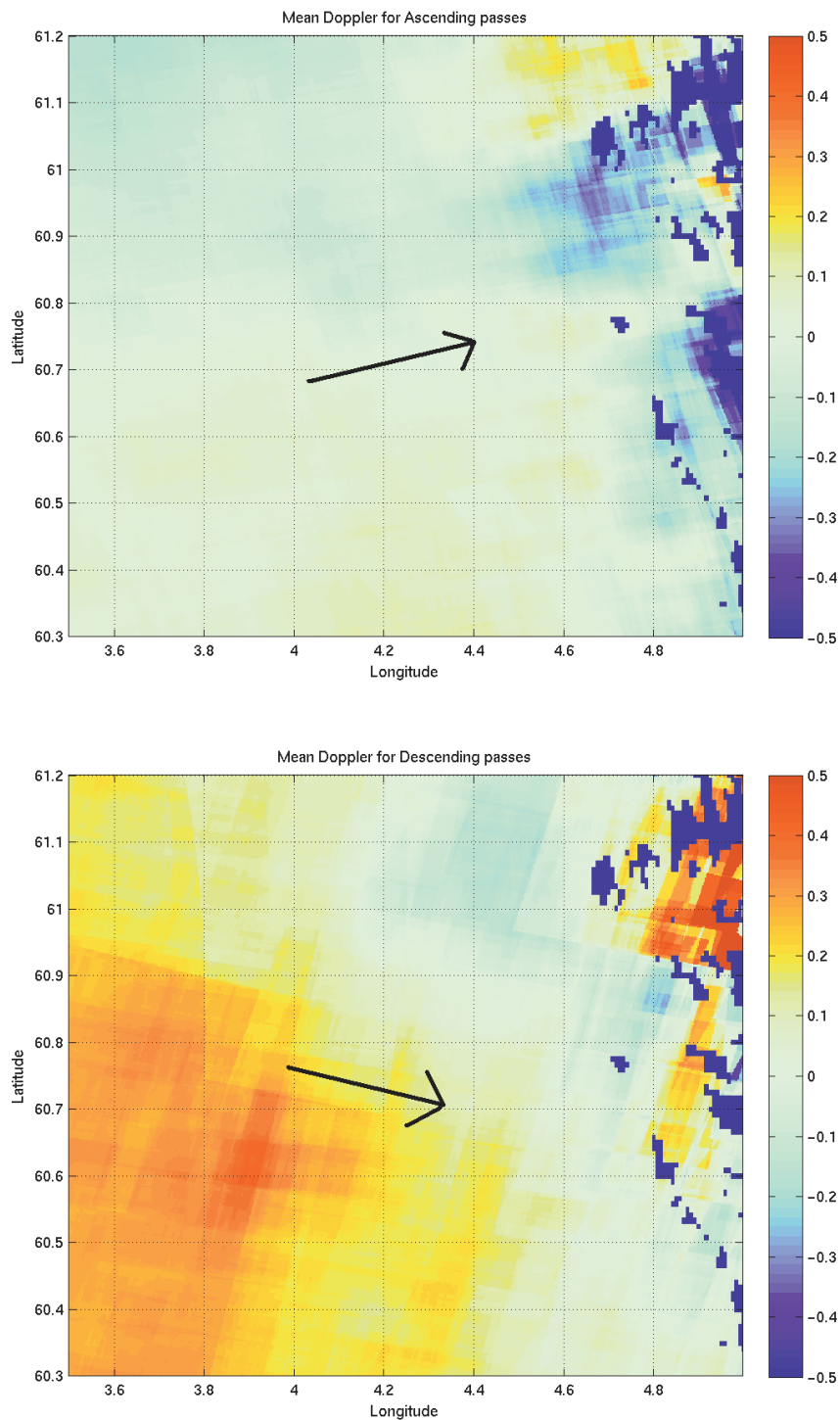
Figure 24: Mean surface Doppler of 50 ascending (upper) and descending (lower) Envisat ASAR scenes from 2008. The angle between the look directions (marked with black arrows) is 2φ=26°.

The corrected ascending and descending Doppler velocities can then be combined into 2-dimensional vectors with the equations:

$$u = \frac{v_{asc} + v_{desc}}{2 \cos \varphi},$$

$$v = \frac{v_{asc} - v_{desc}}{2 \sin \varphi},$$

where u and v are the eastward and northward mean Doppler velocity components, which after correction for wind should correspond to surface currents. The angle between north and ascending and descending satellite passes is $\pm\varphi$, about 13° near Fedje. The combined 2D Doppler velocity field is shown in Figure 25.
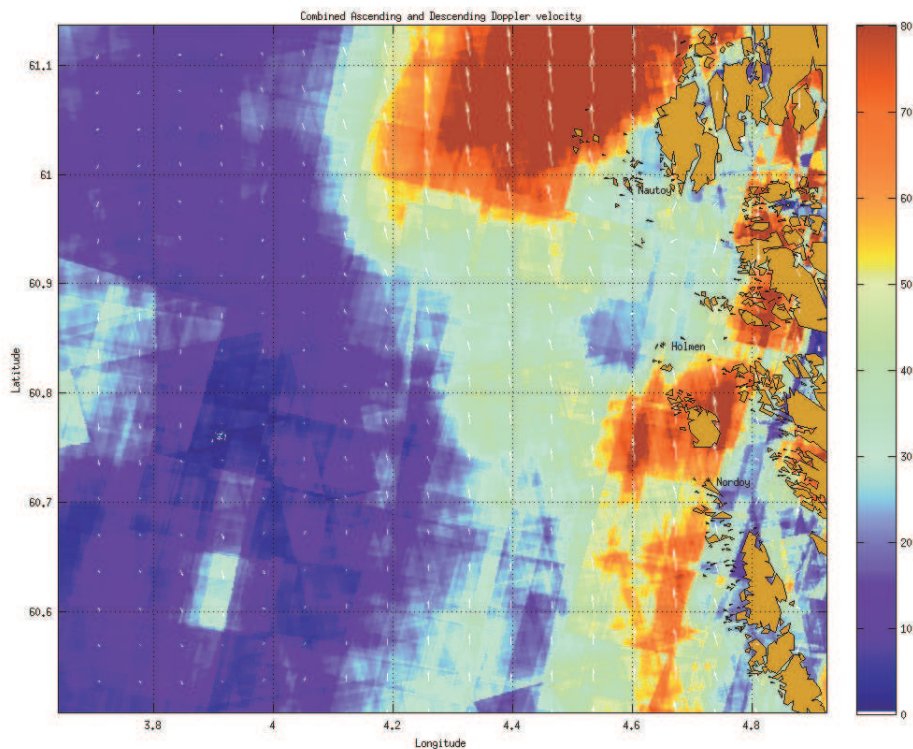
Figure 25: 2D surface Dopper velocity field obtained by combining mean Doppler velocity fields for ascending and descending satellite passes. The contribution from wind has been removed by comparison with the Codar current field, as described in the text. Note that the coverage is slightly larger than for the mean Codar fields shown above.

The reconstructed surface velocity field has qualitative similarities with the mean HF radar current fields. This is encouraging, as quite few SAR scenes have been used, the main current direction is unfavourable, and only a rough correction has been made for the contribution from wind. The obvious strength of the ability to retrieve surface current fields from satellites, compared to in situ measurements, is the possibility to get global coverage at a low cost.

6 Theoretical coverage maps for Lofoten and Finnmark

Theoretical coverage diagrams are presented for the Lofoten area and the coast of Finnmark using two frequency ranges, long range and medium range (see Figure 26-Figure 28). The assumed range using a long range configuration (5 MHz) is 180 km although that can be higher during the day and lower at night. For the medium range configuration (13 MHz) 70 km is the nominal range (with less fluctuation). The ranges can be pushed out a little further with twin transmit antennas and a second transmit chassis to make 70 km into about 95. As can be seen from Figure 27, the Goliat field is on the boundary of medium range standard coverage, hence a long-range system (Figure 28) would be required to ensure adequate coverage of the current conditions around Goliat.

The distance between sites is well suited for long range (about 80 to 90 km separation) as site spacing should be 40-50% of expected range. The local coastline and topography features at any given site may affect the range and radial density coverage. The different colours are for 15° and 30° crossing angles (between the radar beams). Inside 30° crossing angle (pink), the data should be robust. As the angle approaches 15° (coloured red), errors due to poor geometric dilution of precision (GDOP) tend to increase. With the medium range systems, the complex coastline may cause shadowing in certain areas. The cutoff angles are based on the gross coastline features, but local coastline and topography effects (as well as antenna pattern environment) may cause reduced coverage or shadowing. Offshore islands in front of a radar site would have more of an effect at medium range than at long range. The range may go up during the day due to ionospheric conditions.

Radio frequency (RF) background noise has been found to be lower at higher latitudes at most frequencies (leading to better range), but a 5 MHz system has to our knowledge never been operated this far north, so we are not sure what exactly the range would be. The dual transmit and dual chassis configuration is available at both 5 and 13 MHz, but the coverage maps included here are for 13 MHz. Typically, adding a second phased transmit antenna achieves another 10-15% range and driving the second antenna with an additional transmit chassis will increase range by an additional 10-15% again.
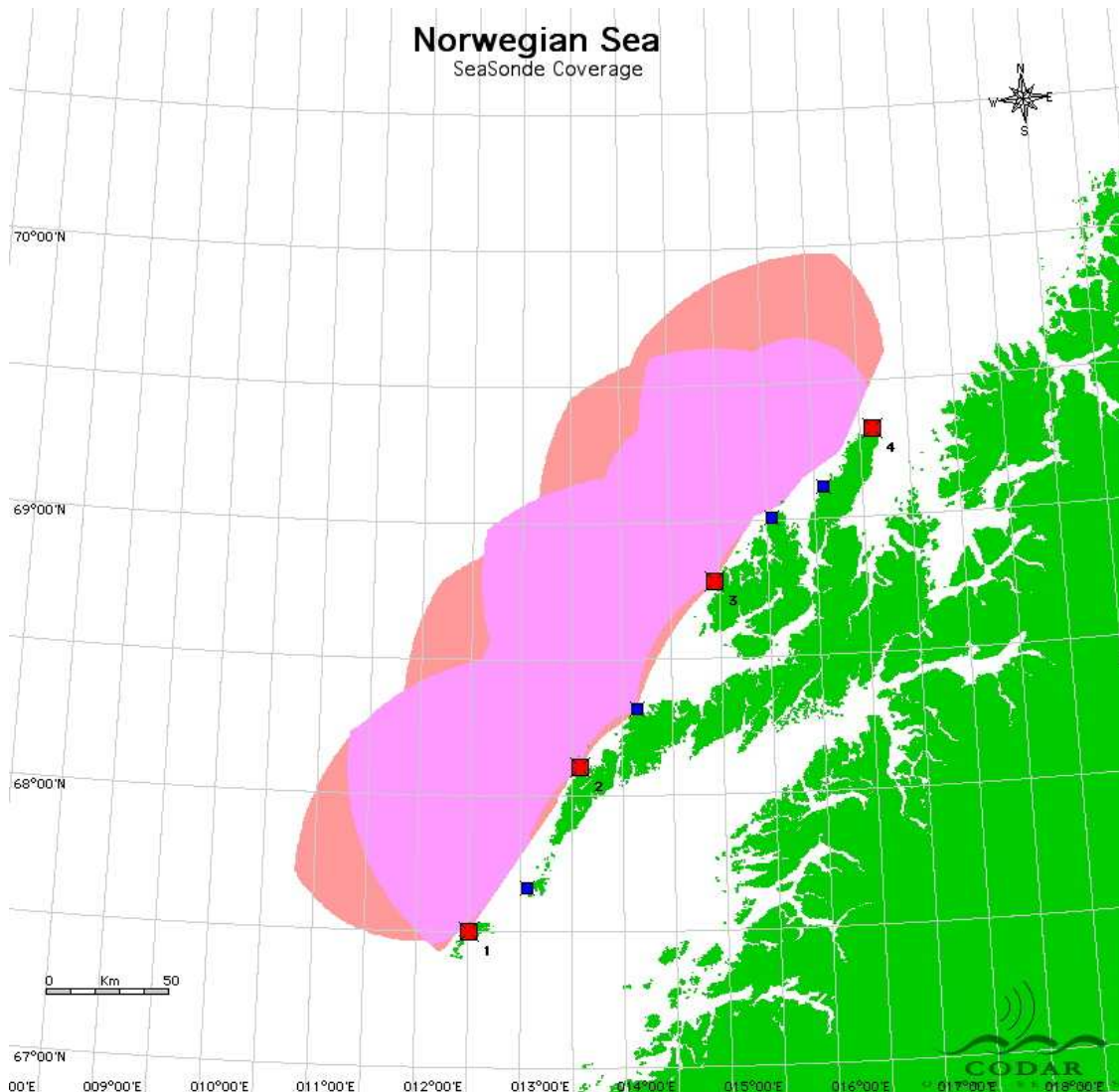
Figure 26: Theoretical coverage using a medium-range HF system in Lofoten. The range goes up with lower frequency, but the spatial resolution goes down.
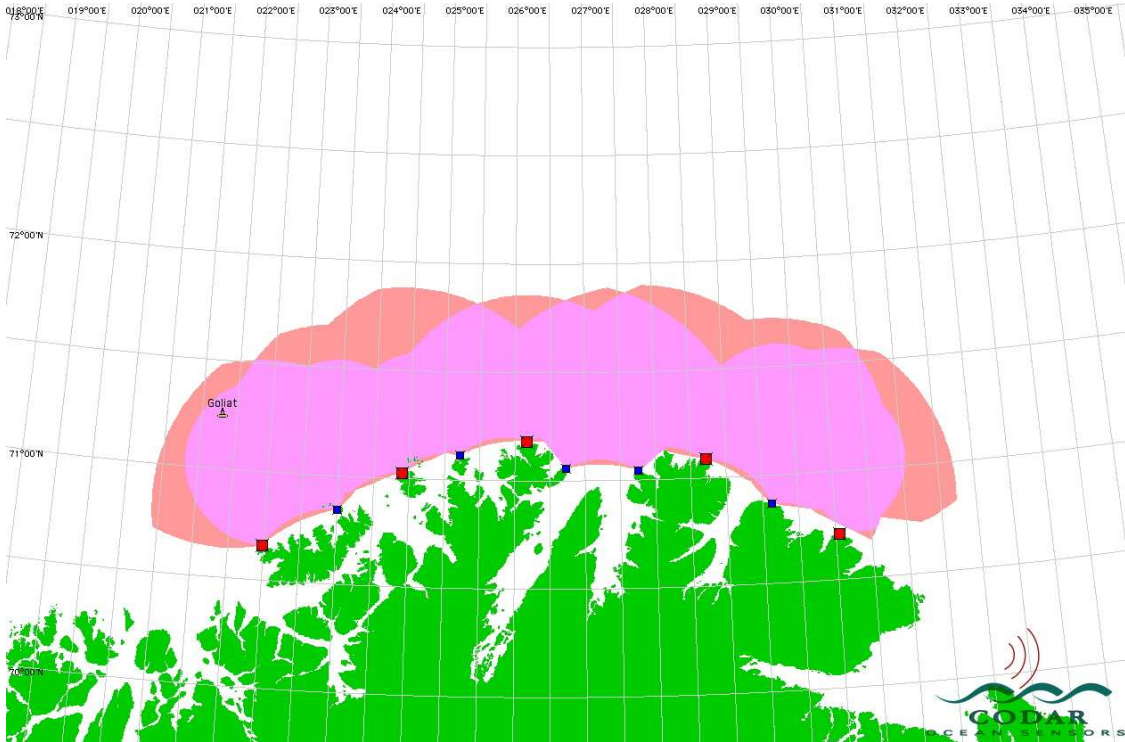
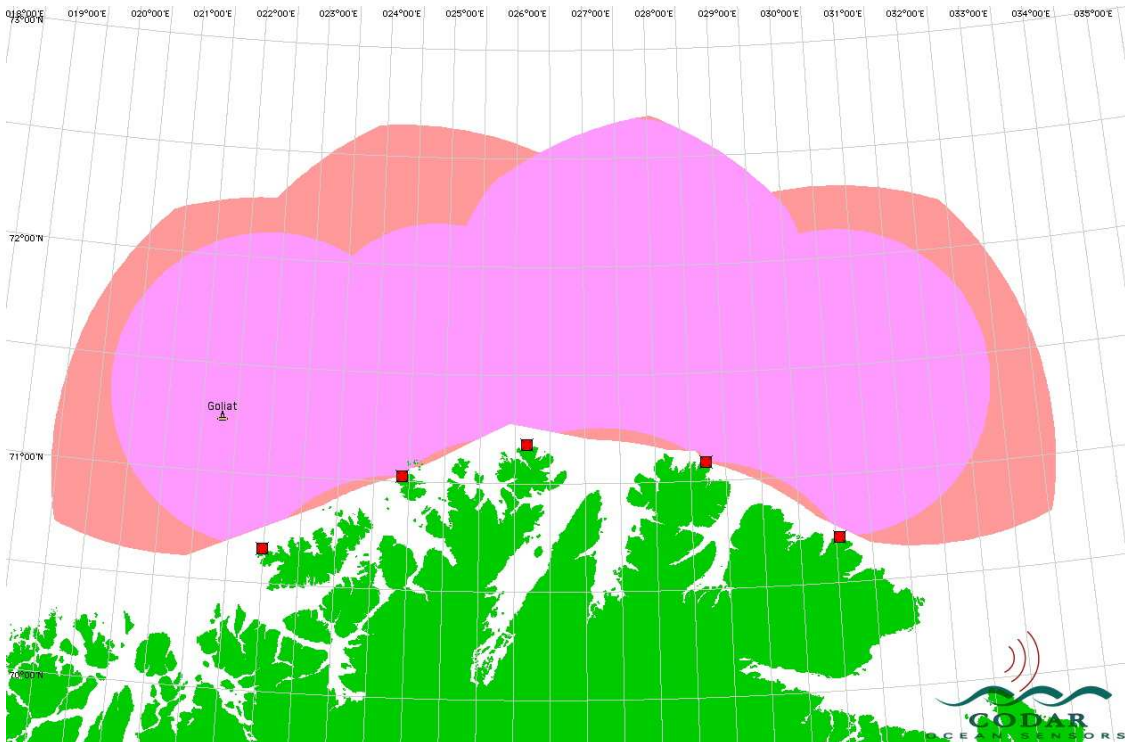**Figure 27: Theoretical coverage using a medium-range HF system in Finnmark.**

Figure 28: Theoretical coverage using a long-range (5 MHz) HF system in Finnmark. This map covers Goliat adequately.

7 Conclusions and recommendations

Averaged HF radar (CODAR) current fields show a persistent northward flow at Fedje with large annual variation in strength. The averaged current fields are smooth, indicating good quality and consistency of the CODAR measurements. The spatial and temporal distribution of speed and direction also looks reasonable.

Comparing current estimates derived from drifters with hourly radar current maps indicates that the mean absolute difference is on the order of 17 cm/s. This is somewhat poorer than the precision reported for the Eastern seaboard of the USA (see Ullmann *et al*, 2006). Comparing the radial current measurements with drifter current vectors decomposed in the direction of the radar yields a more realistic estimate of the precision of the HF radars. We find that the correlation between the radial current measurements and the drifter data is significantly higher than for the total vectors. The Holmen Grå site in particular correlates very well (r=0.90) with the drifter data. We conclude from this that the radars themselves seem to be measuring the surface current well, but the algorithm used to derive total vectors from a linear combination of the nearest radial measurements has certain weaknesses.

Relatively good agreement with drifter tracks from April 2008 is obtained by integrating forward in time using CODAR current fields averaged over about one week. Integration is more unstable using hourly updated CODAR fields for the integration/prediction.

Radar current vectors have also been compared with two (nearly) independent products from the ASAR (Advanced SAR) sensor on the ESA satellite Envisat: traditional roughness images which reveal signatures of current-induced convergence and divergence, and direct surface Doppler velocity measurements in the SAR look direction. For low wind speed, good qualitative agreement is found between HF radar current vectors and the redistribution of surface slicks as observed with ASAR. For moderate wind speeds, currents may be seen in SAR roughness images through modulation of small scale roughness by wave-current and wave-wave interaction. Some qualitative agreement is found for such cases, but there is also some discrepancy, possibly explained by too low spatial resolution of the HF radar, and reduced quality of CODAR vectors along the coverage boundary and between the antennas.

The direct surface Doppler velocities agree in some cases quite well with the HF radar current vectors, although comparison can be made in only one dimension, along the SAR look direction. The area outside Fedje is unfavourable for SAR imaging due to a frequent chaotic wind pattern, and since the coastal current has generally the far strongest component northwards, close to 90º from the typical SAR look directions which are more in the east-west direction.

We conclude that the radars are measuring the surface current with reasonable accuracy, but further work on the algorithm for combining radial vectors into total vectors is recommended. There exist several experimental methods (Kaplan and Lekien, 2007,

Yaremchuk and Sentchev, 2009) for combining the radial vectors where domain-wide constraints on the divergence and vorticity are used to produce a smooth field which is internally consistent. We recommend that for future HF radar installations work is also set aside for establishing such alternative methods for deriving total vectors from the radial measurements. This is work which must be done for each radar installation separately as the coastline, local current conditions and radar coverage will all affect the inversion process.

Theoretical coverage diagrams for potential installations in Lofoten and along the coast of Finnmark have been presented for both medium-range (50-60 km) and long-range systems (~180 km). We recommend a long range system for the coast of Finnmark due to its potential use for monitoring the Goliat site whereas the Lofoten area is better served by a medium-range system due to the complexity of the coastline and the shorter range required to cover the coastal current flowing through the area.

7.1 Operational considerations

Operating an HF radar network requires trained personnel. The Norwegian Coastal Administration (NCA, Kystverket) operate the existing network located around Fedje. One person on site has undergone training by CODAR (the vendor). This appears to be sufficient for operating a network of three radars. Operating more than three radars may require two persons to be trained, although they will not be fully employed operating the network. In general the amount of down-time on an operational (real-time) HF observation network will depend on three factors:

- Availability of trained on-site personnel, preferably on a 24/7 basis
- Accessibility to sites by boat or by road
- Stable power supply and robust communication lines. Additionally, systems for performing remote diagnostics and restart of computers and hardware will reduce the need to physically access the radar sites

As NCA operates an extensive network of lighthouses along the coast the organization is well equipped to operate networks of HF radars, which often tend to be co-located with lighthouses for practical reasons. It is however clear from our discussions with NCA that the cost of operating these networks cannot be covered by NCA. We recommend that an agreement be made with NCA where the cost of operating the network is negotiated.

8 References

Breivik, Ø and Ø Sætra (2001). Real-time assimilation of HF radar currents into a coastal ocean model**,** *J Marine Sys,* **28**(3-4), pp 161-182

Chapron, B., F. Collard, and F. Ardhuin (2005). Direct measurements of ocean surface velocity from space: Interpretation and validation, *J. Geophys. Res*., **110**, C07008, doi:10.1029/2004JC002809

Essen, H-H, Ø Breivik, H Gunther, K-W Gurgel, J Johannessen, H Klein, T Schlick and M Stawarz (2003). Comparison of remotely measured and modelled currents in coastal areas of Norway and Spain, *The Global Atmosphere-Ocean System*, **9**(1-2), pp 39-64

Johannessen, J.A., V.Kudryavtsev, D.Akimov, T. Eldevik, N. Winther, and B. Chapron (2005). On Radar Imaging of Current Features; Part 2: Mesoscale Eddy and Current Front detection. *Journal of Geophysical Research*, **110**, C07017.

Johannessen, J. A., B. Chapron, F. Collard, V. Kudryavtsev, A. Mouche, D. Akimov, and K.-F. Dagestad (2008). Direct ocean surface velocity measurements from space: Improved quantitative interpretation of Envisat ASAR observations, *Geophys. Res. Lett*., **35**, L22608, doi:10.1029/2008GL035709.

Kaplan, D and F Lekien (2007). Spatial interpolation and filtering of surface current data based on open-boundary modal analysis, *J Geophys Res*, **112**(C12), C12007

Ullmann, DS, J O'Donnell, J Kohut, T Fake and A Allen (2006). Trajectory Prediction using HF radar surface currents: Monte Carlo Simulations of prediction uncertainties, *J Geophys Res*, **111**(C12005), DOI:10.1029/2006JC003715

Yaremchuk, M and A Sentchev (2009). Mapping radar-derived sea surface currents with a variational method, *Accepted for publication in Cont Shelf Res*
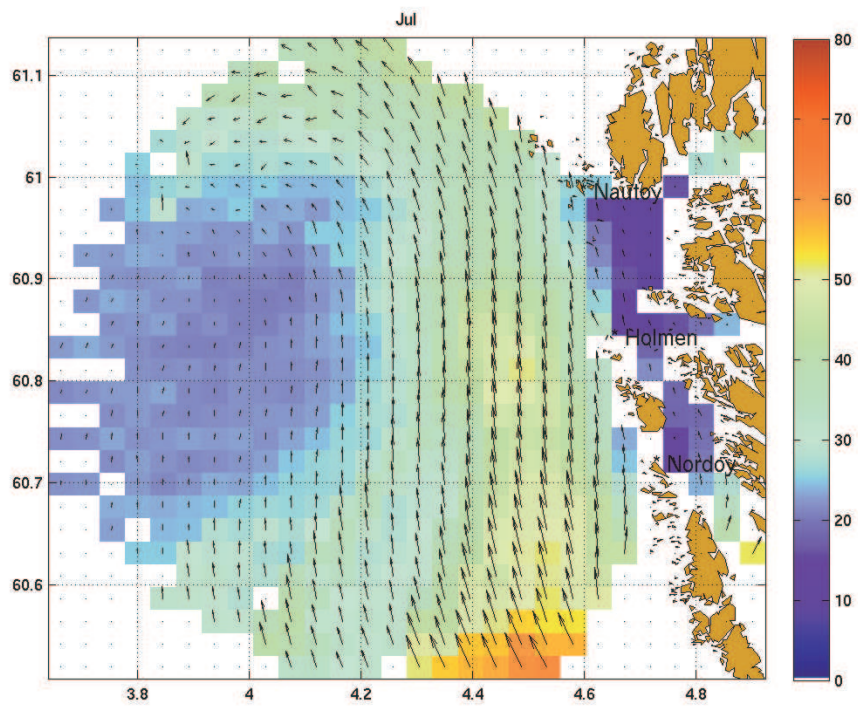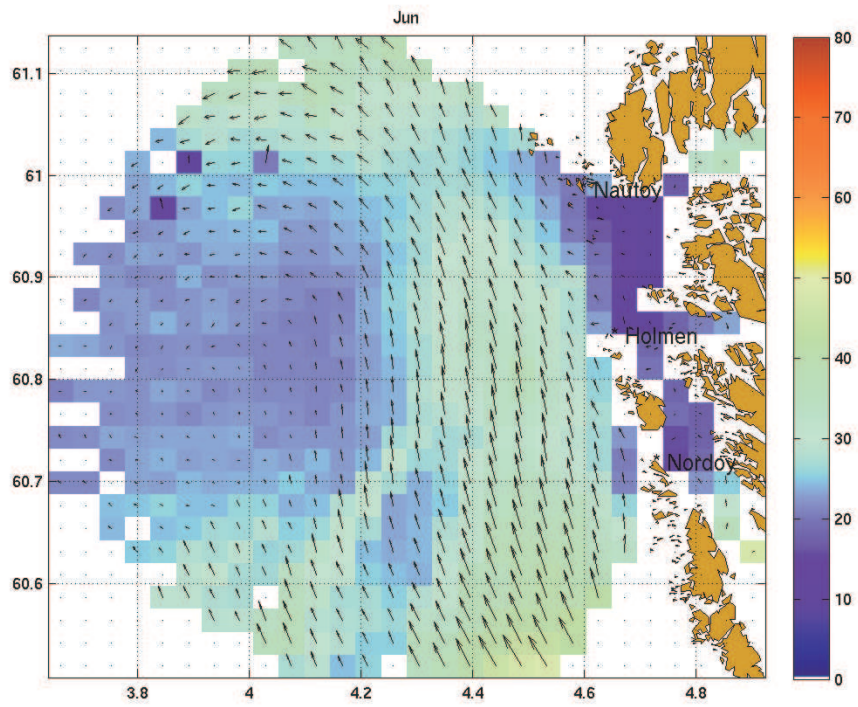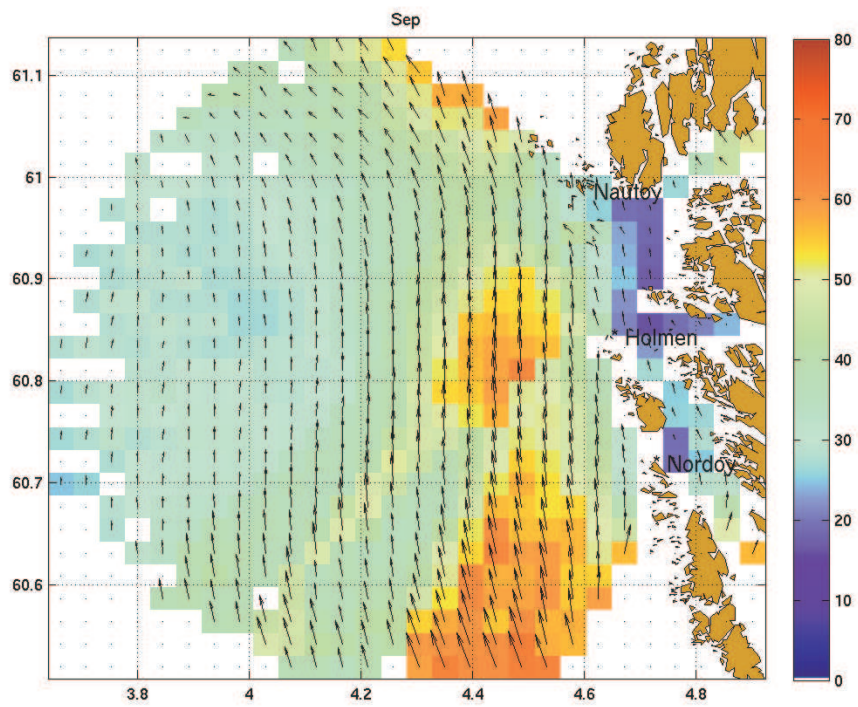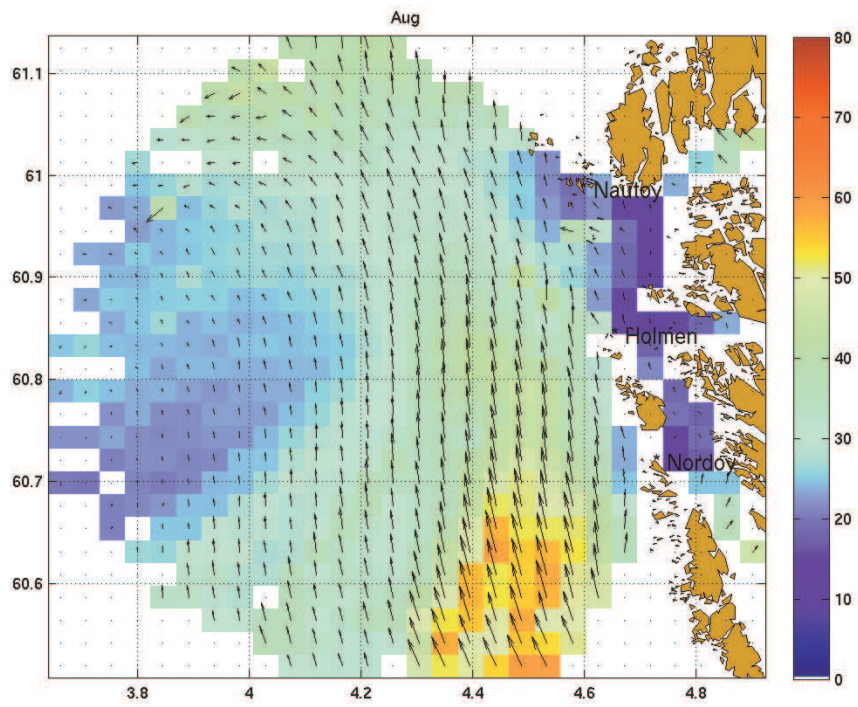
9 Appendix A: Monthly mean HF radar current fields

The following 12 figures show the CODAR current vectors averaged for each of the calendar months. Data from 29 June 2006 to 31 Dec 2008 are used. The averaging procedure is the same as described in Section 2. The scale of the colourbar is cm/s.
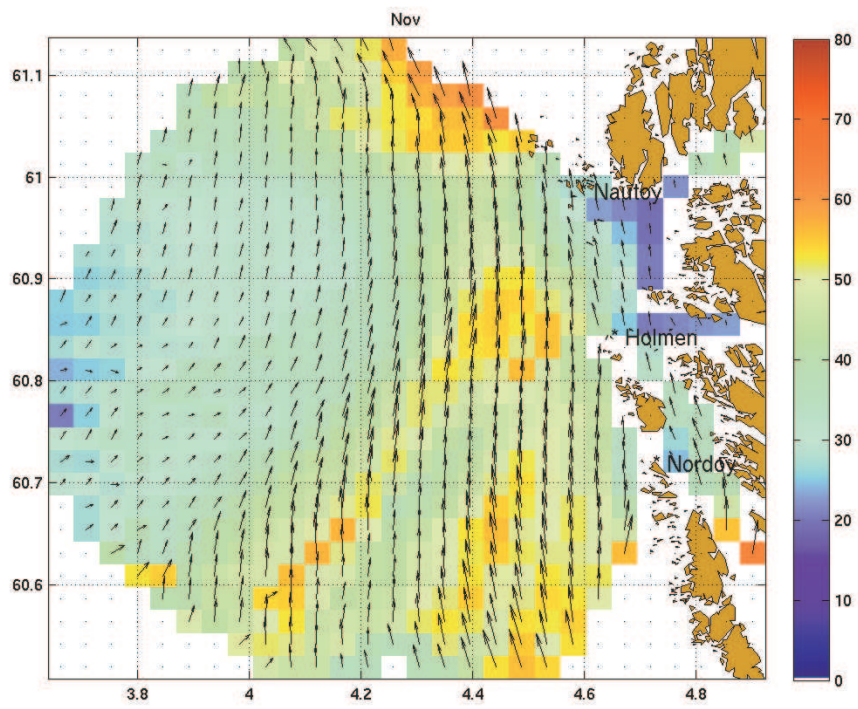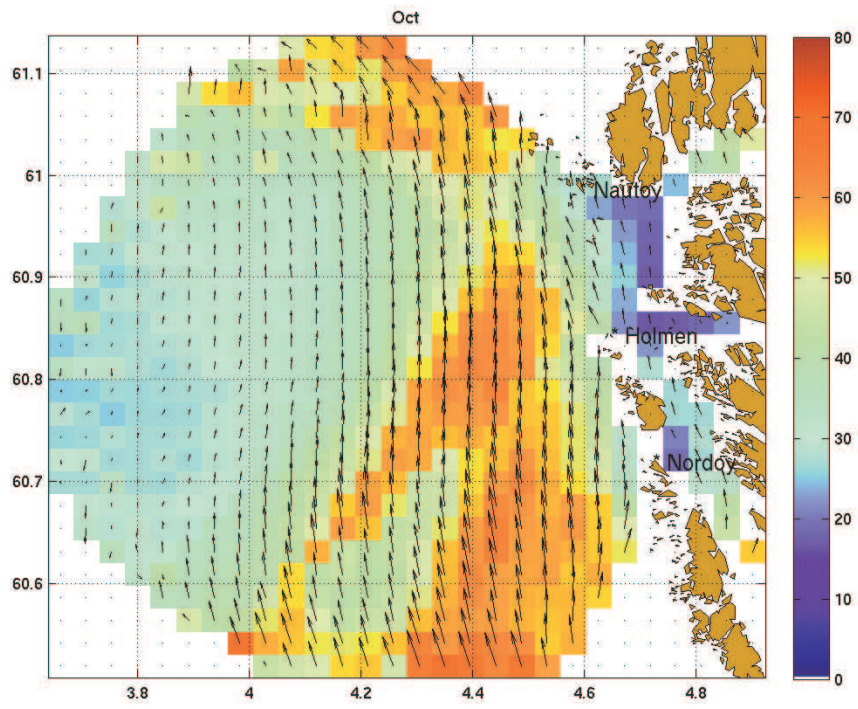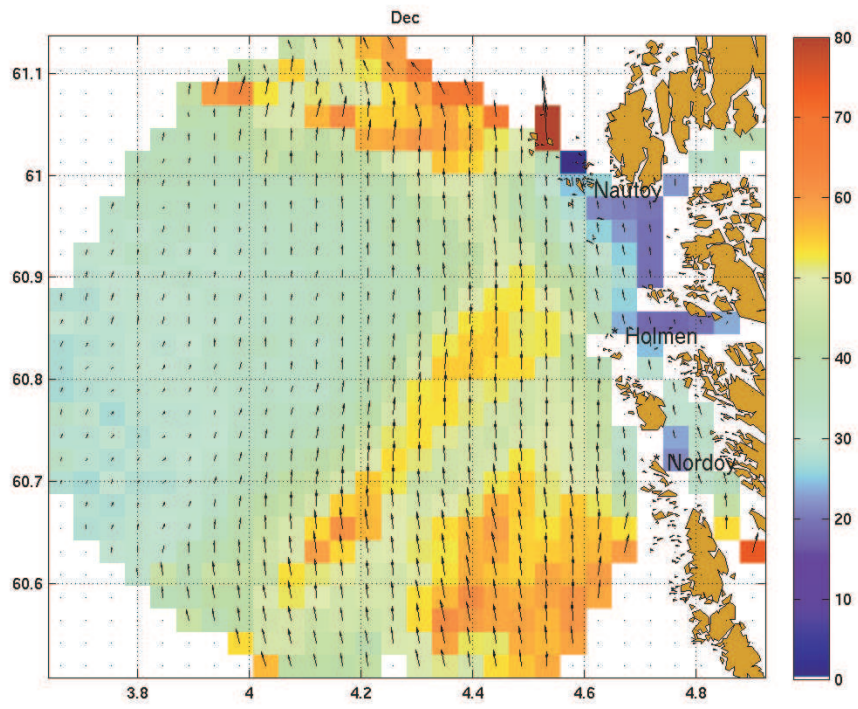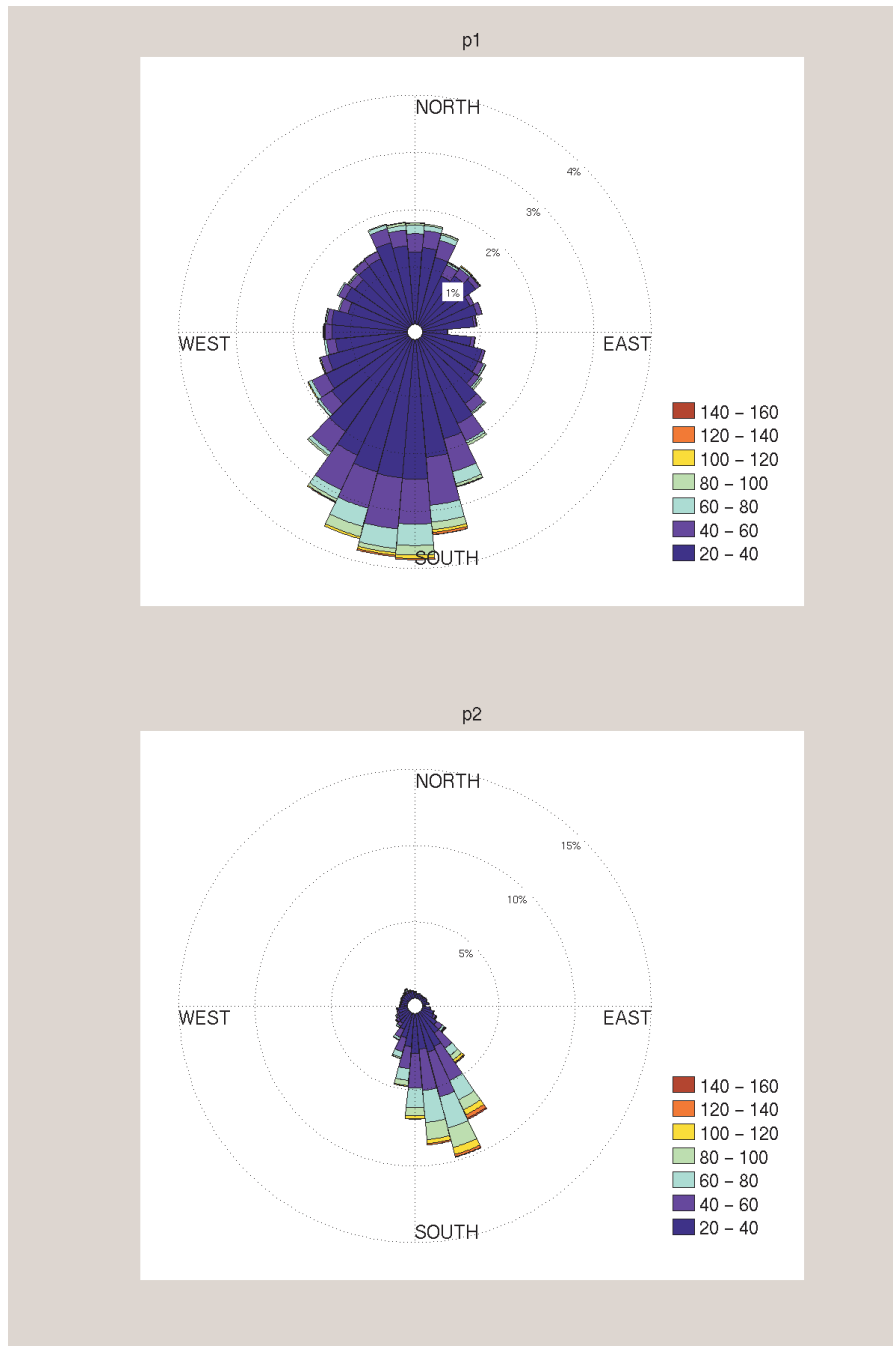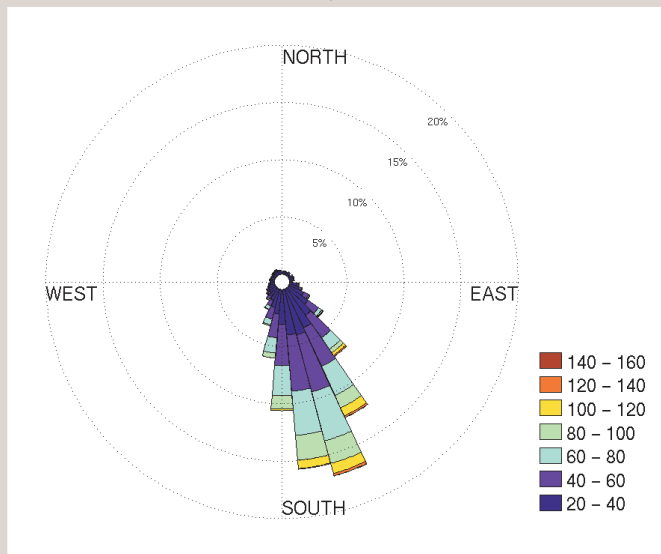
Feb

Mar

Apr

May

Aug

Sep

43

Oct

Nov

Dec
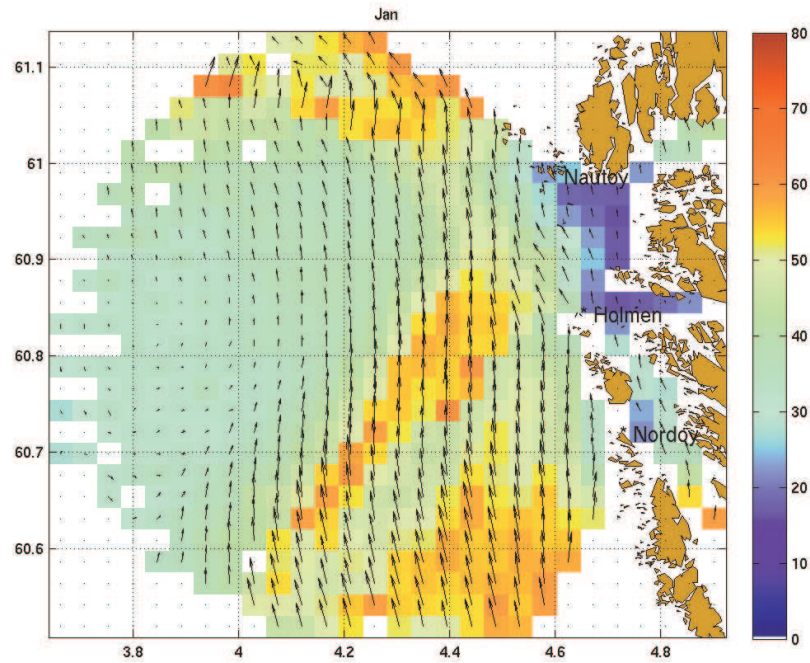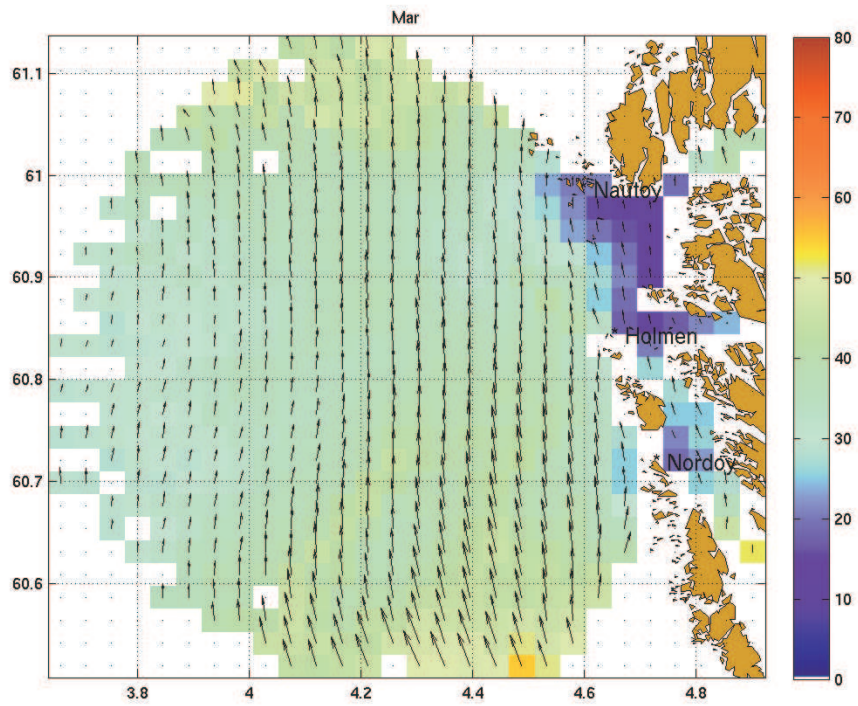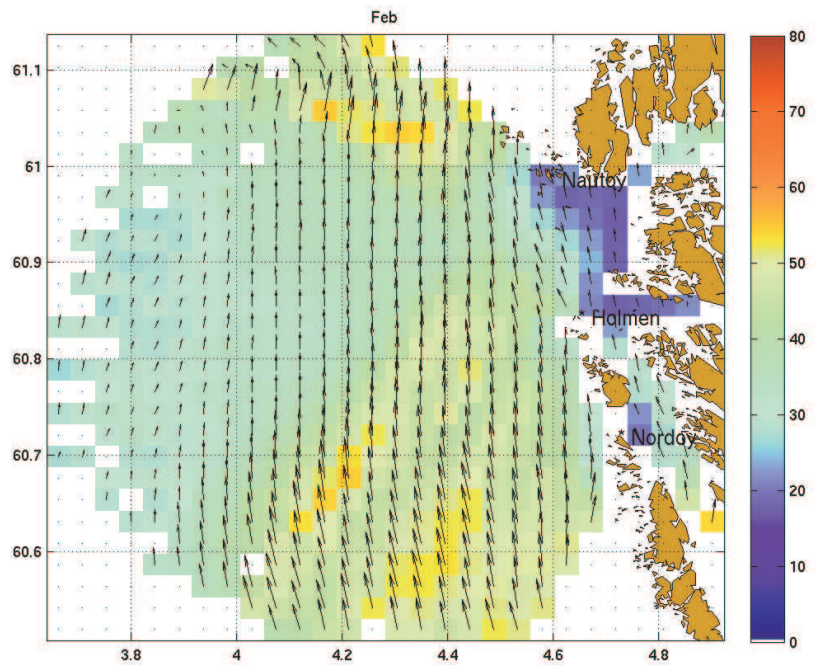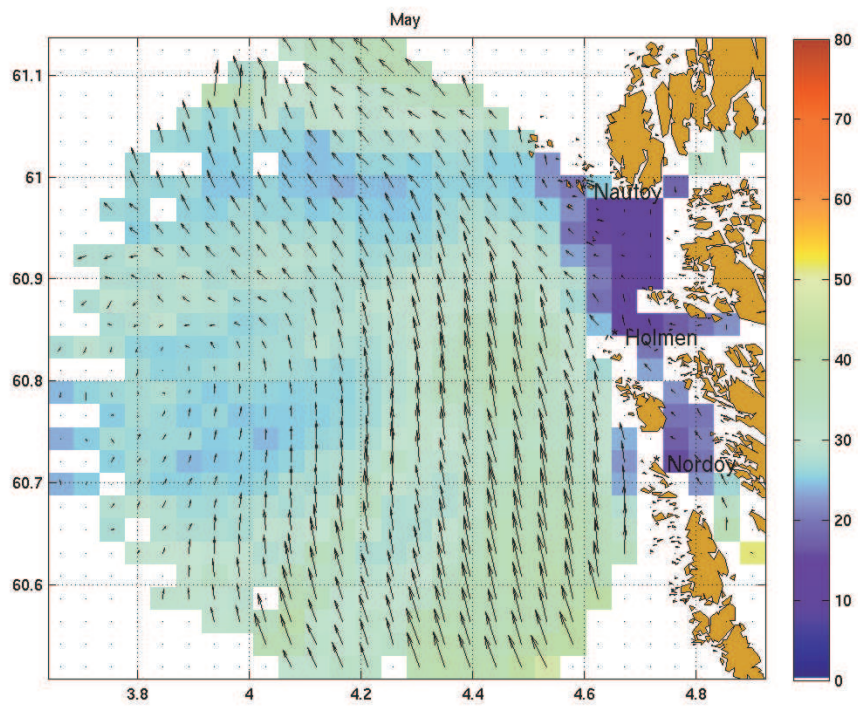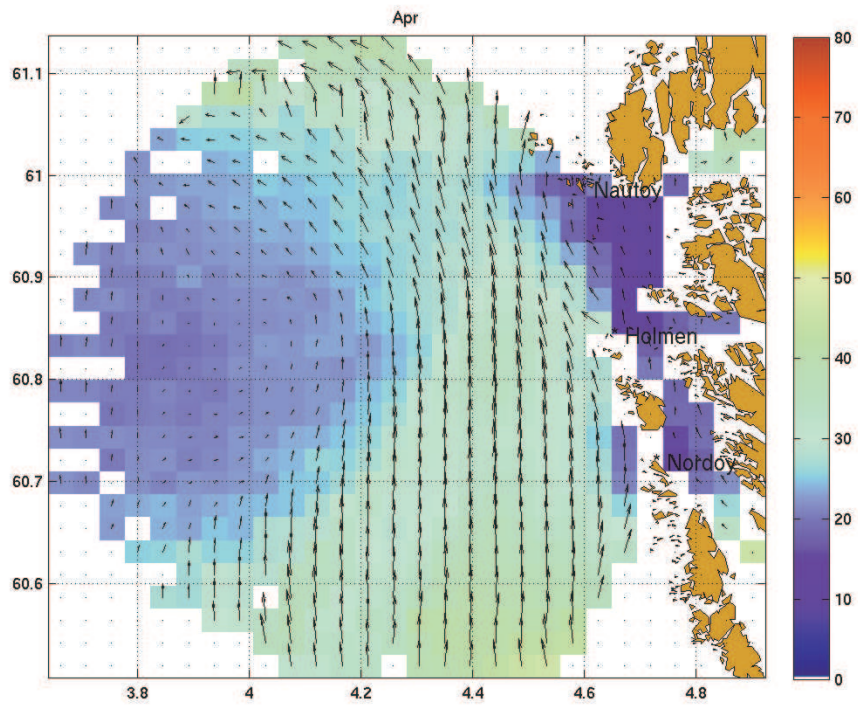
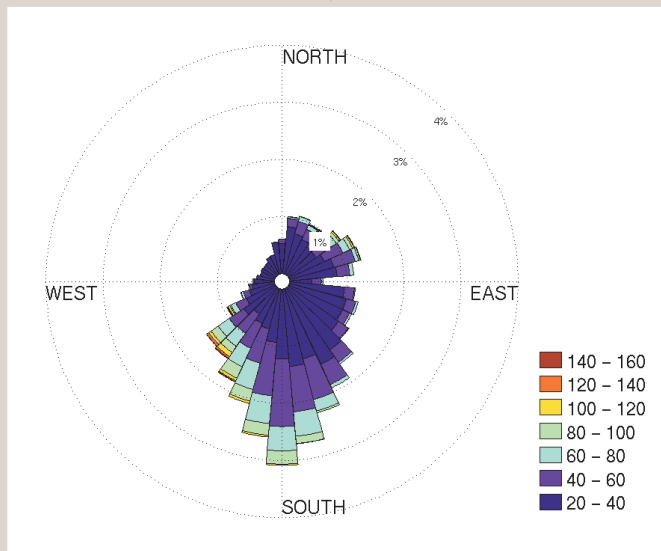# 10 Appendix B: Distribution of CODAR current direction for selected locations

The distributions of CODAR current directions for the 7 locations given in Figure 4 are shown below. The bars indicate the direction from which the current is flowing (meteorological convention).
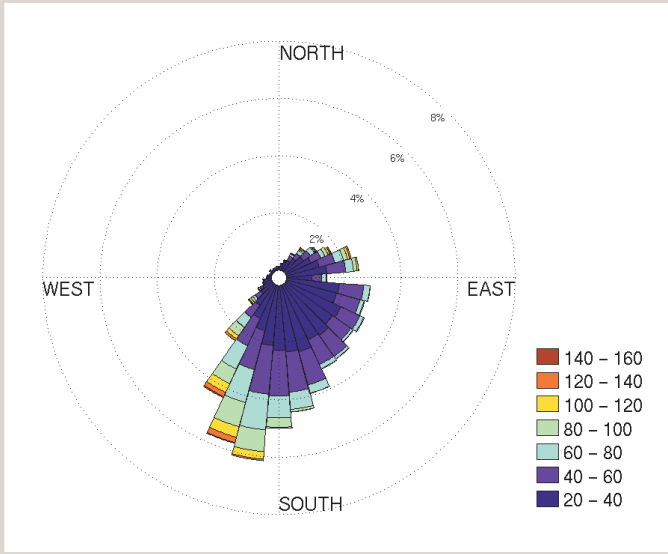
p3

p4

p5

p6

p7